Collapse Of Thick Walled UOE Pipes Corrosive Resistant Cladding

by

JEAN GILBERT LOUIS

THESIS

for the degree of

MASTER OF SCIENCE

(Master i Anvendt matematikk og mekanikk)

Faculty of Mathematics and Natural Sciences
University of Oslo

June 2010

Det matematisk- naturvitenskapelige fakultet
Universitetet i Oslo

Abstract

Current oil exploration depths warrant the need for a better understanding of subsea pipeline collapse capacities. UOE produced line pipe serves as an industry standard, but possess features that can adversely affect collapse capacity. Cladded line pipe are used to prevent internal corrosion of line pipe but may have the ability to contribute to its load carrying capacity.

Necessary concepts and production methods are outlined. Further definition of key factors such as wall thickness, ovality, yield stress and initial circumferential stresses are considered.

Solution methodology involved analytical and finite element solutions. Verification against full scale test data is performed. Analytical solutions are compared and contrasted. Finite element simulations are performed using ABAQUS, including non-linear geometry. Non-linear isotropic material models are implemented, and loading scenarios are based on large deformation theory.

Graphical representation of results is presented together with discussions. The strengthening effect of cladded pipes is apparent, and can help reduce the current wall thickness criterion, which will help line pipe to be dimensioned more accurately.

Acknowledgements

I would like to take the opportunity to thank the following people. Jostein Hellesland at the University of Oslo for his enthusiasm and assistance. Olav Fyrileiv, Bjørn Fallqvist and Jun Liu at the Energy division of Det Norsk Veritas for their support, advice and direction. My loved ones for their relentless support and encouragement. This thesis would not be possible without them.

Contents

List of Figures

List of Tables

Nomenclature

Abbreviations

Item	**Description**
FE	Finite element
CRA	Corrosive resistant alloy
NA	Not applicable
HAZ	Heat affected zone
SMTS	Specified minimum tensile strength
SMYS	Specified minimum yield stress
UO	Pipe fabrication process for seam welded pipes
UOE	Pipe fabrication process for seam welded pipes including the expansion stage
LPF	Load proportionality factor
SAW	Submerged arc welding
DNV	Det Norske Veritas
NS	Not specified
CR	Controlled rolling
TMCP	Termo mechanical controlled process
UR	Unrestrained
ECL	End cap loading
HT	Heat treated
NHT	Not heat treated

Latin Characters

Item	Description
e	Engineering Strain
L_p	Pipe length factor
f_0	Ovality
p	Collapse pressure
A_0	Cross-sectional area at deformed state
A	Cross-sectional area at undeformed state
H	Hardening modulus
E	Young's Modulus
P_{dead}	Pre-load in the RIKS algorithm
P_{tot}	Total load in the RIKS algorithm
p_{atm}	Atmospheric pressure
g	Gravitational constant
P	Applied force
ec	Wall thickness eccentricity
t	Wall thickness
D	Diameter
R	Radius
D/t	Diameter-thickness ratio
h	Depth of submersion
L	Undeformed length

Greek Characters

Item	Description
α_{fab}	Fabrication factor
ε_{lp}	Luder plateau strain
ε	Logarithmic strain
σ	Stress
ν	Poisson's ratio
ℓ_r	Arc length in the RIKS algorithm
λ	Load proportionality factor in ther RIKS algorithm
ρ	Density
β_{inf}	Angle of influence
β	Ovality as a scaling factor
ℓ	Deformed length

Subscripts

Item	**Description**
o	Outer
i	Inner
pl	Plastic
el	Elastic
z	Axial direction
r	Radial direction
θ	Circumferential direction
n	Nominal
t	Total
y	Yield
yo	Offset yield
res	Residual
e	Effective
hyd	Hydrostatic
h	Hoop (circumferential) direction
bs	Backing Steel
cra	Internal cladding
c	Collapse
tr	Transition
exp	Experimental
an	Analytical

Chapter 1

Introduction

Global oil dependancy has resulted in a growing need for the production of oil. Most subsea oil extraction currently takes place on relatively shallow waters. Increasing demand has deemed viable the drilling of oil at ultra deep levels. Warranting a deeper understanding of production methods, loading scenarios, and failure modes associated with ultra deep pipeline operations. Collapse or local buckling describes the failure mode that is critical for deep water applications. A non-linear analysis will replicate the actual problem with greater accuracy. Geometric imperfections will be examined together with different material models. This will hopefully increase understanding and knowledge pertaining to subsea line pipe.

The added strengthening effect of an internal corrosive resistant alloy is usually not taken into account when determining collapse capacity. The potential increase in collapse capacity will be investigated numerically and compared to monolithic data.

Imperfections implemented will be a natural result of the UOE production process. A fully non-linear analysis will be performed using a finite element package. Comparisons to current offshore standards and available experimental findings will be made.

Chapter 2 examines the key concepts that need to be understood before delving further into the nature of the problem. Certain conventions will be established and kept consistent throughout the thesis. Chapter 3 looks at the UOE manufacturing process, turning plates into tubulars. The necessity for a cladded line pipe is explored together with loading situations that arise during installation and operation. Chapter 4 considers the cur-

rent standards for assessing collapse capacity. Essential components of the analytical solutions will be evaluated and deemed viable for numerical implementation. Simplifications and assumptions will be covered, including numerical algorithms that are central to the solution scheme. Chapter 5 decribes the definition of parameters contained within the finite element model. Implementation of the numerical scheme will be covered, together with mesh density and comparison to full scale test data. Chapter 6 serves as a further refinement of simulation methodology. The vast amount of numerical data will be represented graphically to enable discussions. Chapter 7 serves as a final impression of the works presented combined with the potential for further work in the field.

Chapter 2

Fundamental Concepts and Modes of Collapse

2.1 Motivation

This section serves as a brief introduction into the key concepts and terminalogy used throughout the thesis, which is also necessary for a reader to be familiar with in order to fully understand the material presented.

2.2 Coordinate Systems

An intelligent choice of coordinate system can help save time when undertaking large studies. Considering the geometric nature of pipe sections, it seems natural to use a cylindrical coordinate system. The standard three dimensional cartesian coordinate system, (x, y, z), is transformed to a cylindrical coordinate system, (r, θ, z).

Figure 2.1 shows the visual relationship between the two coordinate systems. Naturally the pipe segment's length would be oriented parallel to the z axis. The mapping equations are presented as.

$$x = r\cos(\theta)$$

$$y = r\sin(\theta)$$

$$z = z$$

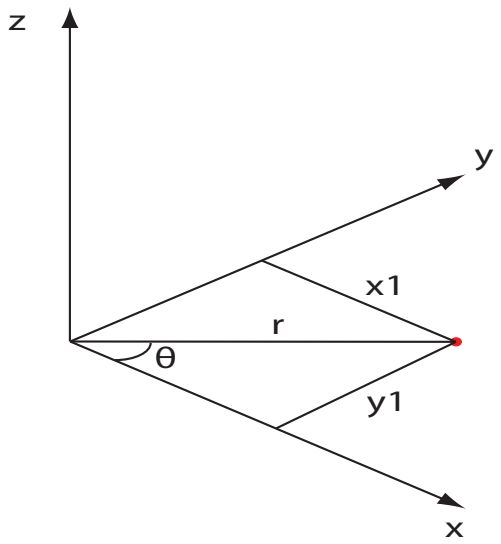

Figure 2.1: Relationship between cartesian and cylindrical coordinate systems.

Geometric data pertaining to the pipe segment can now be input using radial, circumferential and axial dimensions.

2.3 Choice of Units

Considering the nature of the problem and the relative magnitudes of displacements and forces, it seems much more natural to operate in what is refered to as SI millimeter units. A summary over this is presented in table 2.1

Quantity	SI Units	SI Units (mm)
Length	Meters (m)	Millimeters (mm)
Force	Newtons (N)	Newtons (N)
Mass	Kilograms (kg)	Kilograms (kg)
Stress	Pascals (Pa)(N/m^2)	Mega Pascals (MPa)(N/mm^2)
Density	(kg/m^3)	(kg/mm^3)

Table 2.1: Summary of Unit System.

From this point on, all dimensions will be declared in SI millimeter units.

2.4 Logarithmic Strain

Engineering strain as a measure is better suited for problems with small strains. Logarithmic strain can also be referred to as the true strain or natural strain, which is better suited for problems where the loading takes place in step increments, and where large deformations occur.

The one dimension definition of engineering strain is give in euation 2.1.

$$e = \frac{\Delta L}{L} = \frac{\ell - L}{L} \tag{2.1}$$

Where L is the original length and ℓ is the final length.

Considering the definition of incremental logarithmic strain yields equation 2.2.

$$\partial\varepsilon = \frac{\partial\ell}{\ell} \tag{2.2}$$

Integrating the expression results in equation 2.3

$$\begin{aligned} \int \partial\varepsilon &= \int_L^\ell \frac{\partial\ell}{\ell} \\ \varepsilon &= [\ln(\ell)]_L^\ell \\ \varepsilon &= \ln(\ell) - \ln(L) \\ \varepsilon &= \ln(\frac{\ell}{L}) \end{aligned} \tag{2.3}$$

Subsituting the expression for the engineering strain gives equation 2.4.

$$e + \frac{L}{L} = \frac{\ell}{L}$$

Equation 2.5 shows a useful relation as a result.

$$\frac{\ell}{L} = 1 + e \tag{2.5}$$

Substituting gives the final expression as equation 2.6.

$$\varepsilon = \ln(1 + e) \tag{2.6}$$

2.5 Bifurcation

Bifurcation is a mathematical term used widely in the field of structural mechanics. It is a critical point along a load displacement curve that has two equilibrium states simultaneously. This kind of behaviour is very typical for buckling problems indicating a sudden change in the shape of the structure followed by negative stiffness in the load displacement curve. It is important to mention that strain energy is released during this region of negative stiffness where the 'snap-through' behaviour is observed.

It is necessary to make the distinction between a standard axially loaded struts response, and the expected collapse behaviour.

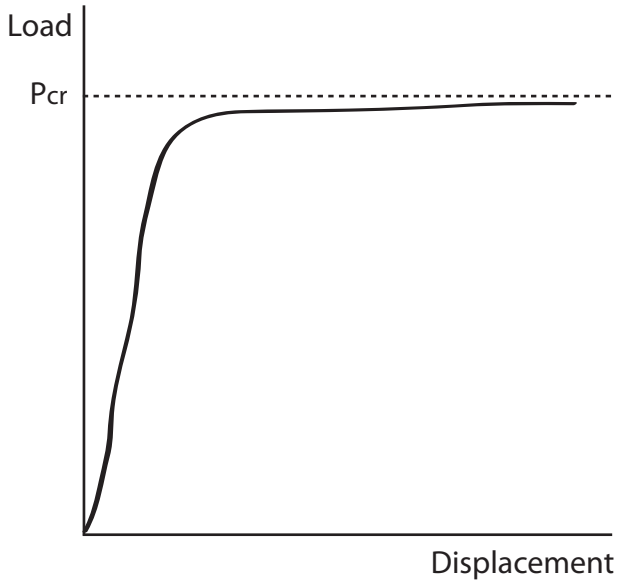

Figure 2.2: Typical Euler strut buckling response.

Figure 2.2 shows the actual load-displacement response of an Euler strut up to the critical buckling load. This is not the linearised idealisation and displays post-buckling response which is not the nature of collapse problems.

Figure 2.3 shows the load-displacement response for a typical collapse problem. The response of the system can be characterised into several parts.

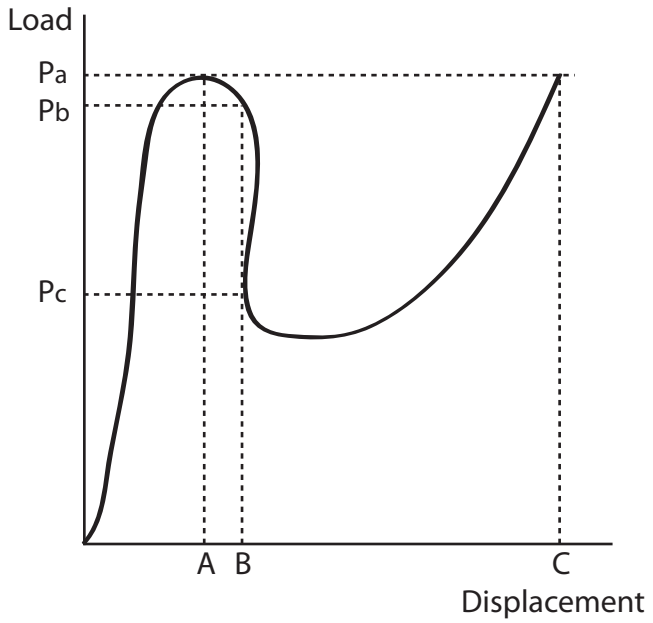

Figure 2.3: Typical response for collapse problems.

The response tracked from load level zero up to point P_a yields a displacement response from zero up to point A. This region can be compared to the corresponding part of the curve from figure 2.2 and usually displays a fairly linear behaviour. The load level P_a can be called a critical buckling point and is generally considered the maximum load when looking at problems of a collapse nature.

The response is now tracked from load level P_a to P_b which yields a further displacement from point A to point B. This region can be refered to as the bifurcation region. At displacement level B, there is in fact 2 load levels that permit equilibrium, namely, P_b and P_c. It is clear that in this region the response displays a negative gradient, indicating negative stiffness. This means that this region then characterises the actual collapse or snap-through of the system. Load level P_b can be referred to as the bifurcation point, possessing all the necessary features to describe it as such.

The response tracked from load level P_c back to P_a yields a further displacement from point B to point C. This region is known as the post-buckling response of the system and shows an increased carrying capacity which is dependant on boundary or contact conditions that allow the system to be further loaded. This region is not relevant for the analysis of a collapse problem.

The differences between these two failure modes is evident and helps generate

the necessary knowledge for collapse based problems.

2.6 Local Buckling and Collapse

The load-displacement response of typical collapse problems have been introduced in section 2.5. This section will look at how these terms as related to an actual pipe segment.

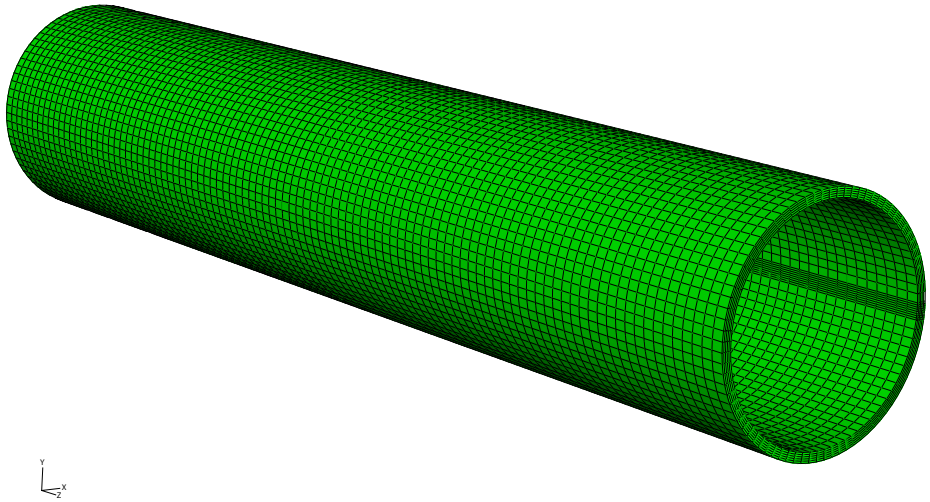

Figure 2.4: Undeformed view of the pipe segment

Figure 2.4 shows an undeformed pipe section. Orientation is placed with respect to a cylindrical coordinate systems decribed in section 2.2. The axial dimension of the pipe is alligned with the z axis.

Local buckling is defined as the buckling mode confined to a short length of the pipeline causing gross changes of the cross-section[9]. Figure 2.5 shows the collapsed state of the pipe segment.

Figure 2.6 shows a cross-section of the pipe segment in its collapsed state. This does not represent the maximum load P_a at corresponding displacement A depicted in figure 2.3. Instead this represents a much further progression along the load displacement curve.

Figure 2.7 shows the actual load-displacement curve for the collapsed models shown in figure 2.5 and figure 2.6. The maximum load level is the peak attained in figure 2.7, which will be the load level used to defined the collapse pressure of the pipe segment.

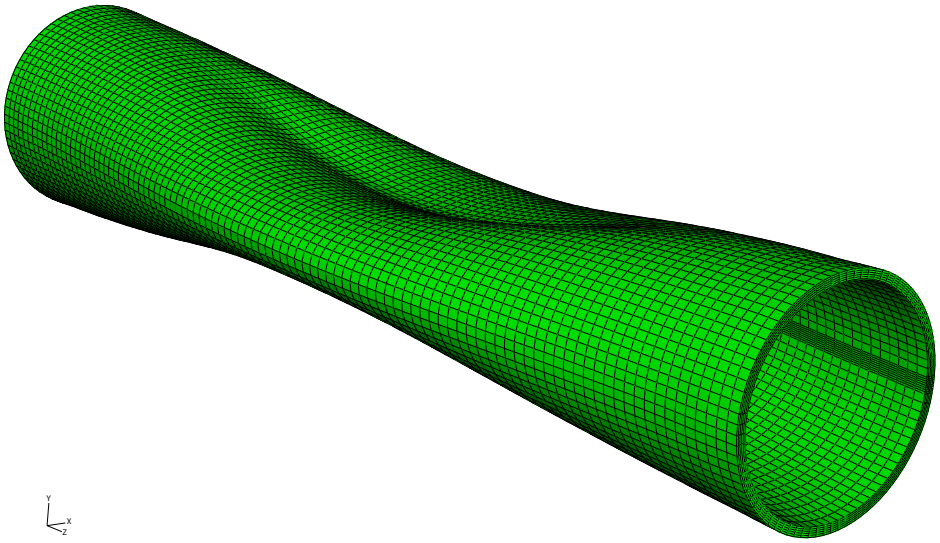

Figure 2.5: Deformed view of the collapsed pipe segment

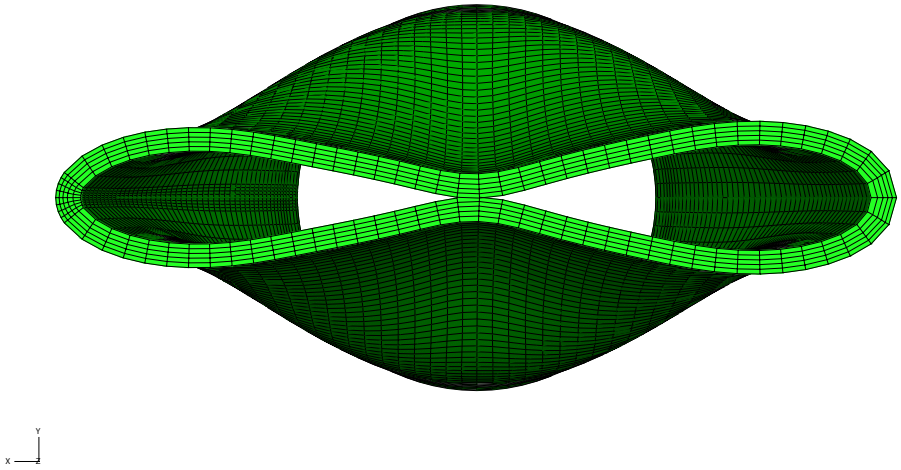

Figure 2.6: Cross-sectional view of the collapsed pipe segment

2.7 Linear VS Non-Linear

2.7.1 Fundamentals

Linearised theory makes certain assumptions that would be in strong violation of these type of collapse problems. These assumptions are as follows.

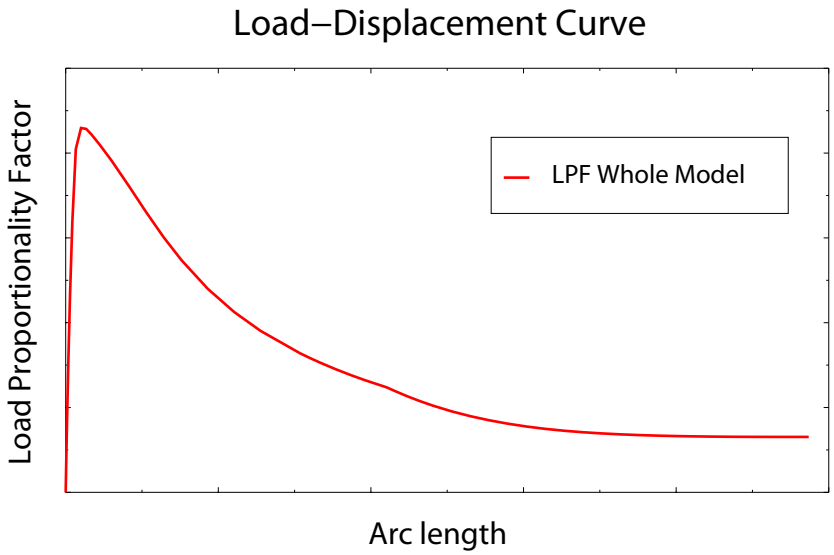

Figure 2.7: Load-Displacement curve for collapse

- Small deformations- Linear geometry, implementing the assumption that for small angles $\sin(\theta) \approx \theta$.

- Linear kinematics- assumming that loads and boundary conditions act in relation to the structures undeformed geometry.

- Linear material behaviour- indicating a linearly elastic distribution of the stress-strain curve.

Collapse problems possess a feature that the structure's stiffness and kinematic conditions are dependant on the displacements and deformations of the system. Therefore one must allow for numerical formulations to account for large deformation and displacements, essentially non-linear geometry and kinematics.

Material properties can be formulated linearly, but considering the nature of carbon steel, material non-linearity is also implemented.

2.7.2 Kinematics

Kinematics can be loosely defined as the task of keeping track of the structures displacements and deformations. This involves the structures boundary conditions, loading patterns, and contact conditions as all of these factors are directly related to altering the structures displacement and deformation. The constituitive equations needed to maintain equilibrium of the structure, need to be formulated using large deformation theory. Most FE packages allow for such analyses and conditions to be performed.

2.7.3 Geometry

The geometrically non-linear assumption takes into account the deformed configuration of the structure when formulating each successive load increment. The solution then becomes history dependant and in order to reduce any errors generated during the iterative scheme, the time steps should be kept small. This also ensures that strains and rotations are sufficiently small at each time step so that equilibrium equations can be developed accurately. History dependant effects must be modelled correctly ensuring an accurate response of the system to the specified loads.

2.7.4 Material

A materials stress-strain response is crucial in a non-linear study and therefore necessary to define the relevant terms.

Figure 2.8 displays the typical stress-strain response exhibiting metal plasticity. The curve consists of three distinct regions.

The first region, denoted by the red curve in figure 2.8, is the linearly elastic region. It has a constant gradient throughout this region which is equivalent to the materials Young's modulus. This can be calculated as given in equation 2.7

$$E = \frac{\sigma_y}{\varepsilon_y} \tag{2.7}$$

Where ε_y is defined as the corresponding strain at the yields stress, σ_y. Loading and unloading in this region results in zero permanent plastic deforma-

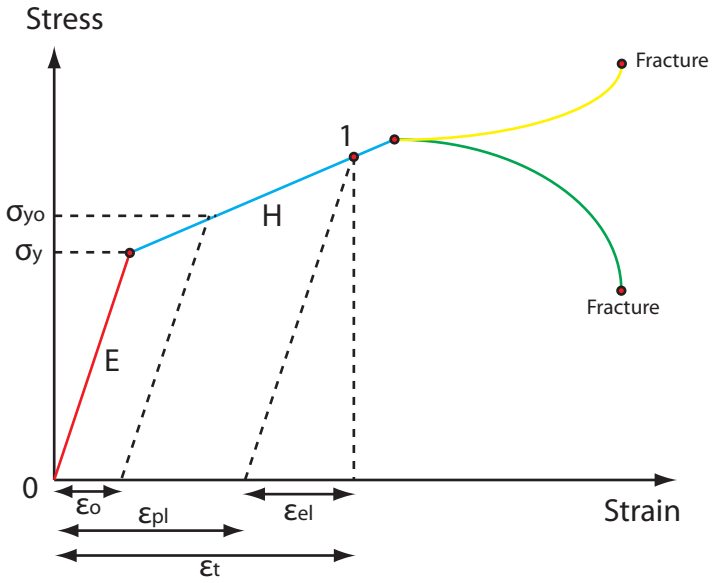

Figure 2.8: Key terms for non-linear material behaviour.

tion. The stiffness of the metal typically decreases dramatically once the material yields.

The second region, denoted by the blue curve in figure 2.8, is the plastic region of the curve. This region does not need to be linear, but certain material models apply this condition. The gradient of this region is defined by a hardening modulus, H, which is usually taken as a fraction of the materials Young's modulus. Any material loading and unloading in this region will result in permanent plastic deformation. Strain hardening is a term usually associated with this region of the curve and is indicative of the materials ability to sustain further stresses during plastic deformation.

The final region, denoted by the green and yellow curves in figure 2.8, is the failure region. The green curve represents the nominal stress response and the yellow curve represents the true stress response of the material. The major distinction between these two stresses can be exemplified by considering a simple uniaxial tension test. Upon reaching the final region of the material's stress-strain curve, necking is usually observed prior to fracture. Necking implies that the specimens cross-sectional area starts to reduce substantially, and it is this feature that introduces these different stress interpretations.

Nominal stress is defined in equation 2.8.

$$\sigma_n = \frac{F}{A} \tag{2.8}$$

A is defined as the initial cross-sectional area of the specimen. Essentially nominal stress readings do not account for any reduction in the cross-sectional area as the material begins to neck.

True stress is defined in equation 2.9.

$$\sigma_{true} = \frac{F}{A_0} \tag{2.9}$$

A_0 is defined as the cross-sectional area at the time that the particular load level is applied. The true stress therefore accounts for changes in the cross-sectional area.

Conservation of volume for an incompressible material yields equation 2.10

$$\frac{A_0}{\ell} = \frac{A}{L} \tag{2.10}$$

Inserting equation 2.10 into equation 2.9 gives the expression in equation 2.11.

$$\sigma_{true} = \frac{F}{A_0} = \frac{F\ell}{AL} = \sigma_n \left(\frac{\ell}{L}\right) \tag{2.11}$$

Applying equation 2.5 from section 2.4, equation 2.11 can be simplified to equation 2.12.

$$\sigma_{true} = \sigma_n(1 + e) \tag{2.12}$$

In the first two regions of the materials stress-strain response, cross-sectional area reduction is not as evident as in the final region leading upto failure. This is why the deviation between nominal and true stress is much more apparent in the final region. Most finite element packages require that material data be declared in true values rather than nominal, emphasising the importance of this concept.

The zero offset yield stress, σ_y, in figure 2.8 can also be interpreted as a limit of proportionality. This essentially means that σ_y is the maximum stress

such that all strain can be recovered upon unloading. The offset yield stress, σ_{yo}, however defines the yields stress with a predefined offset strain, denoted ε_{yo}. An offset yield stress will allow a certain amount of plastic deformation during loading. Usually ε_{yo} is chosen to be 0.2 percent, indicating that the magnitude of this permitted plastic deformation is relatively small.

Considering point 1 in figure 2.8, the plastic, elastic and total strains are shown. Their relationship is established in equation 2.13

$$\varepsilon_t = \varepsilon_{pl} + \varepsilon_{el} \tag{2.13}$$

Ductility is a measure of how much a material can deform plastically prior to fracture. This is essentially a measure of the strain hardening region combined with the failure region as depicted in figure 2.8. A ductile metal that has yielded will recover its initial elastic stiffness when the applied load is removed.

Chapter 3

Manufacturing and Pipe Laying

3.1 Steel Production

The current varieties of subsea pipeline are most typically made from carbon steel.

The production of subsea pipelines have become a major industry due to rapid growth in the oil industry[7]. The massive cost of production and transportation of oil has resulted in the development of a niche when it comes to pipe production. Pipeline production has some of the most stringent requirements when it comes to its mechanical properties. Desireable qualities include

- high strength
- high ductility
- high toughness
- high corrosion resistance
- good weldability

During the production process there is a high degree of monitoring during each phase of the production process to ensure tight specifications. There are several types of non-destructive testing methods performed during production such as; ultra sonic, magnetic and x-ray testing. These methods will detect any imperfections, or weld defects that may arise during production.

Tubulars can be either seamless or seam-welded. Seamless pipes are generally used for diameters up to 16 inches or 400 mm, and seam-welded pipes are generally used for diameters upto 64 inches or 1600 mm. There are 3 main steps taken to improve the material properties of steel.

Basic metallurgy states that steel is a polycrystalline material[7]. The crystals contain small defects known as dislocations, which is the main mechanism that limits the strength of the material. When these dislocations move, the material then experiences plastic deformation. The steel is however strengthen through several chemical processes, resulting in increased resistance of motion for these dislocations.

Solid solution hardening is the process of adding impurities to form an alloy[7]. These impurities help to prevent the motion of these dislocations and hence increase the stress required for them to deform plastically, ultimated increasing the material yield stress, σ_y.

One of the most important processes for steel strengthning is grain (crystal) size refinement[7]. The polycrystals yield strength is inversely proportional to the square root of the grain size, therefore a smaller grain size would also result in a higher yield stress.

Plate production is the first step for seam-welded tubulars after the steel has been properly treated. Increasing demand for thick walled pipes have improved the production requirements for casting and hot rolling of these plates into tubulars. Plate making has evolved into an advanced field, consisting of multiple stages during the production process. Basic requirements for plates are as follows.

- Steel is free from impurities and contains low levels of carbon and sulphur.
- Precise microalloying in order ensure uniform mechanical properties.
- During the rolling process temperatures should be uniform and well controlled.
- Cooling should be applied uniformly.

All of these requirements are hard to attain perfectly, but it is important that the manufacturer is aware of tolerances that are acceptable in order to maintain the right grade of steel.

The rolling process has a relatively significant effect on the isotropy of the plate, especially with respect to yield stresses in certain directions. Rolling along the length of the plate encourages grains to allign in the rolling direction. This will result in a lower longitudinal yield stress than the yield stress in the transverse direction. There is also some variation in yield stress through the thickness of the plate, due to varying rates of cooling through the thickness. The top of the plate generally has the highest yield stress, the mid-thickness has the lowest yield stress and the bottom of the plate has a thickness averaged yield stress[7]. Variations in yield stress when considering, longitudinal, transverse and thickness directions can vary as much as 20% for relatively thick plates[7].

3.2 UOE Production Process

The UOE process is the primary production method for pipe diameter in excess of 16 inches. It is important to mention that the steps that transform the plate into a tubular are cold forming processes.

Figure 3.1 presents the key stages of the UOE production process, turning plates into tubulars.

First the edges of the plate are crimped into circular arcs. The U press then further forms the distinct U-profile. The plate is then subjected to a O-press. The plate has now been almost completely transformed to a tubular. The longitudinal seam is then welded using a SAW process. It is important to note that the seam is welded from the inside and the outside. The final stage involves a mechanical expansion of the welded pipe. This is to ensure the pipe displays circularity within the given tolerances. The expansion stage of the forming process can be omitted, then being called a UO pipe instead.

UOE pipe manufacturing using X65 grade steel can produce the following range of dimensions[7] given in table 3.1.

The axial length range is not a continuous range, but rather one or the other. Cold forming of thick-walled tubulars means that the shorter of the two length choices must be made as the forming equipment is unable to handle the maximum thickness for the longer pipe section. A lower bound for the diameter to thickness ratiohas been established which will assist in defining the scope of the numerical simulations.

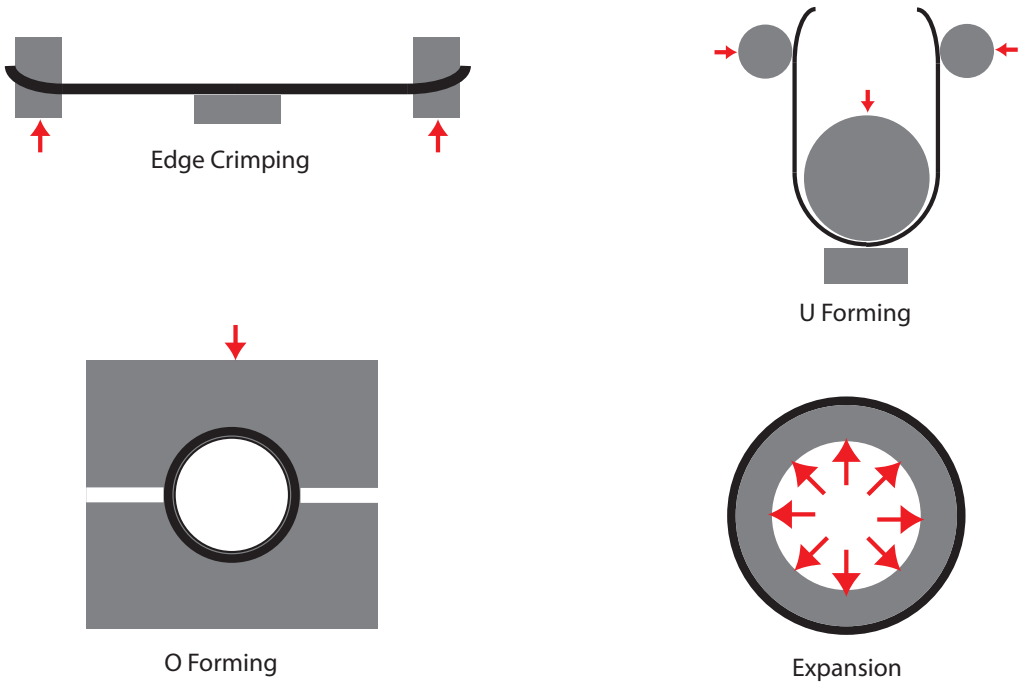

Figure 3.1: Four stages of the UOE forming process.

3.3 Cladded Pipes

Pipelines are often coated internally with a corrosive resistant alloy. The mechanism that holds the CRA in place can either be metallurgical or mechanical. A metallurgical bond implies that the CRA layer is welded to the pipe segment when it is still in its plate form, usually refered to as a cladding. A mechanical bond indicates that the CRA is prepared as a tubular first, then inserted into the pipe segment and expanded, usually refered to as a liner. The scope of this thesis will extend to the case of an internal cladding.

Clad pipe is defined as a pipe with an internal corrosion resistant liner where the bond between the backing steel and cladding material is metallurgical[9]. Figure 3.2 shows a cross-sectional view of the pipe depicting the cladding and the backing steel. The thickness of the cladding, t_{cra}, is much smaller than the thickness of the backing steel, t_{bs}. This allows the assumption of thin-wall behaviour when pertaining to the internal cladding.

Dimension	Minimum	Maximum
D_o (mm)	406.4	1625.6
L_z (m)	12.2	18.3
t (mm)	NA	44.5
D/t ratio	≈ 10	NA

Table 3.1: Range of Dimensions for seam welded pipes.

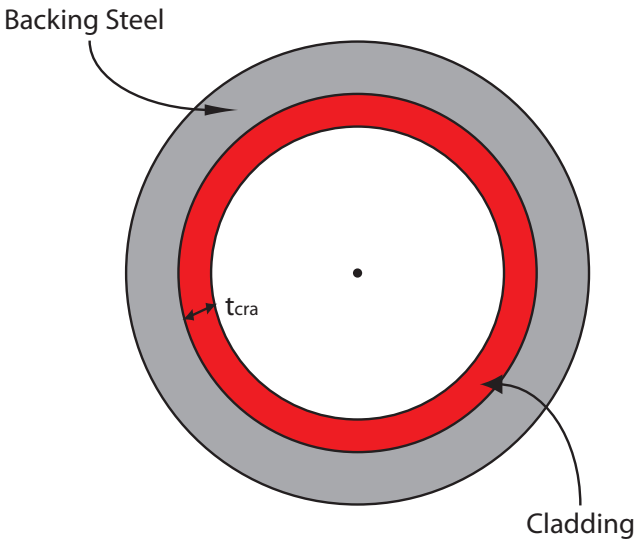

Figure 3.2: Pipe cross-section depicting the internal cladding

The internal cladding is also subject to the cold forming UOE processes used to form the tubular. Stainless steel is more flexible than the backing steel and is also much thinner, implying that any residual stresses built up in the CRA may be neglected.

It is assumed that the CRA layer is in perfect allignment with the backing steel and the two layers are in perfect contact throughout the plates surface area.

3.4 Pipe Laying Methods

The process of laying the pipe on the seabed can introduce loading situations that are only present during the laying process. The primary loading condition considered in this thesis will be when the pipe is already submerged and subject to pure hydrostatic pressure.

Purely Hydrostatic Loading

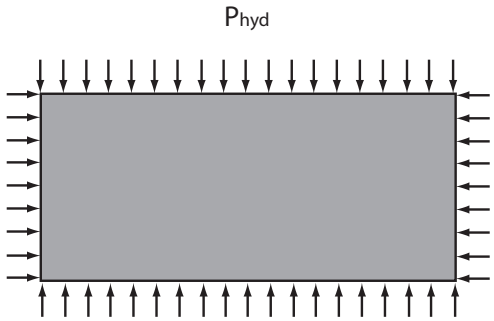

Figure 3.3: Axial view of the pipe section subject to pure hydrostatic loading.

Figure 3.3 shows the loading situation when the pipe segment is laying on the seabed.

Moment, Tension and Hydrostatic Loading

S-Lay

This is the method of pipe laying where the laying vessel is feeding the pipe in a horizontal direction. This results in the characteristic S-shape.

Point 1 in figure 3.5 represents the purely hydrostatic loading situation depicted in figure 3.3. Point 2 in figure 3.5 represents the mixed loading situation depicted in figure 3.4.

J-Lay

This is the method of pipe laying where the laying vessel is feeding the pipe in a vertical direction towards the seabed. The result is the characteristic J-shape.

Point 1 in figure 3.6 represents the purely hydrostatic loading situation de-

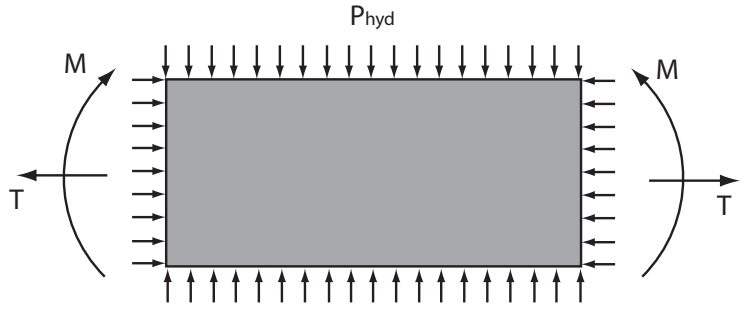

Figure 3.4: Axial view of the pipe section subject to hydrostatic, moment and tension loading.

picted in figure 3.3. Point 2 in figure 3.6 represents the mixed loading situation depicted in figure 3.4.

It is important to be aware of the different loading situations so that further research can be performed within the field. Considering the more complex loading scenarios will give more reliable insight into the collapse capacity of thick-walled pipes.

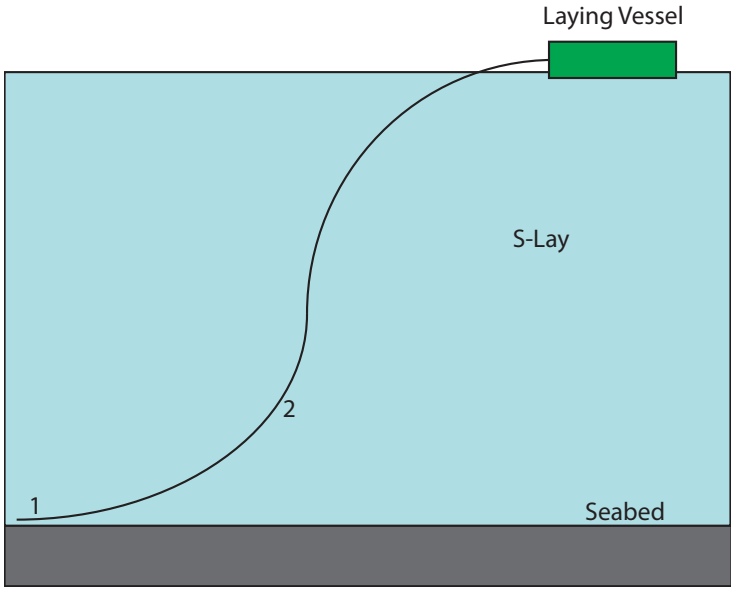

Figure 3.5: S-Lay schematic.

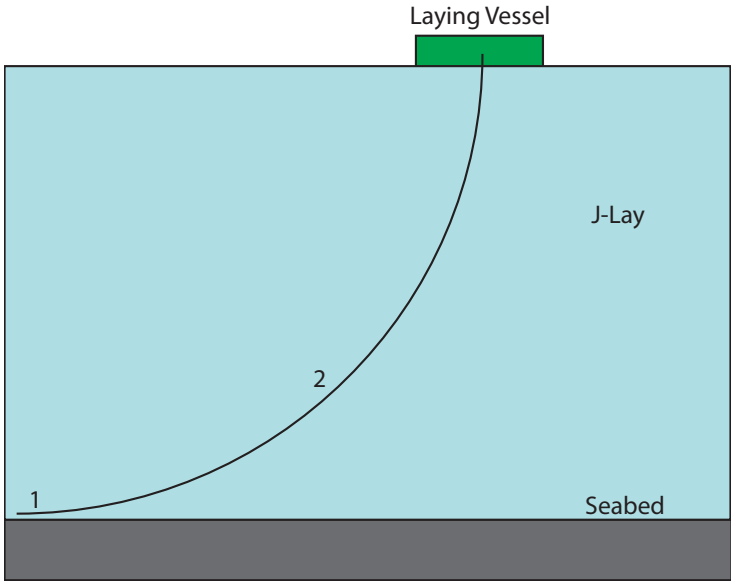

Figure 3.6: J-Lay schematic.

Chapter 4

Analytical Procedures

4.1 Motivation

This section will cover the analytical process necessary for a greater insight of the collapse problem. Important sections of [9] will be extracted and implemented in this section. Analytical collapse equations will be evaluated and their interactions will be dicussed. Key parameters of the pipe segments collapse capacity will be assessed on its pertinence to implementation over to numerical methods.

4.2 DNV Offshore Standard

Det Norske Veritas (DNV) have produced an offshore standard (DNV-OS-F101) that pertains to submarine pipeline systems. This handbook is intended as a guide for designers and engineers that require verification from DNV. It covers all activities specific to subsea pipelines with defintions, limit state equations, loading scenarios and material requirements considering different methods of production. Section 4.5 will be used to present the limit state equations, but first certain concepts need to be clarified.

Nominal plastic strain increment shall be calculated from the point where the material stress-strain curve deviates from a linear relationship[9]. This corresponds with the definition presented in section 2.7.4.

The yield stress is defined as the stress at which the total strain is 0.5%[9].

Based on terms defined in section 2.7.4, and offset yield stress, σ_{yo}, with an offset strain, $\varepsilon_{yo} = 0.005$.

Possible beneficial strengthening effect of cladding on a steel pipe shall not to be taken into account in the characterictic resistance, unless the strengthening effect is documented[9]. The cladding material thickness shall not be less than 2.5 mm[9]. This means that the minimum cladding thickness is enforced for its corrosion resistance and not its strengthening effect. This will serve as a lower bound during the numerical simulations.

4.3 Geometric Definitions

It is necessary to define the geometric variations that constitute part of the analytical collapse equations.

A pipe segments wall thickness is usually defined by a dimensionless quantity refered to as the D/t ratio.

$$D/t = \frac{D_o}{t_n} \tag{4.1}$$

It is important to note that the D/t ratio shown in equation 4.1 is calculated based on the pipes outer diameter, D_o. Relevant dimensions are depicted in the figure 4.1.

The pipe segments ovality, f_0, is a crucial parameter of the collapse pressure. This is presented in equation 4.2, and depicted visually in figure 4.2. Sometimes the ovality may be represented as a percentage in which case f_0 is simply multiplied by 100. The ovality must have a minimum value of 0.005[9].

$$f_0 = \frac{D_{max} - D_{min}}{D_n} \tag{4.2}$$

It is important to note that the ovalised cross-section must have the same wall thickness circumferentially in order to not induce any wall thickness eccentricity.

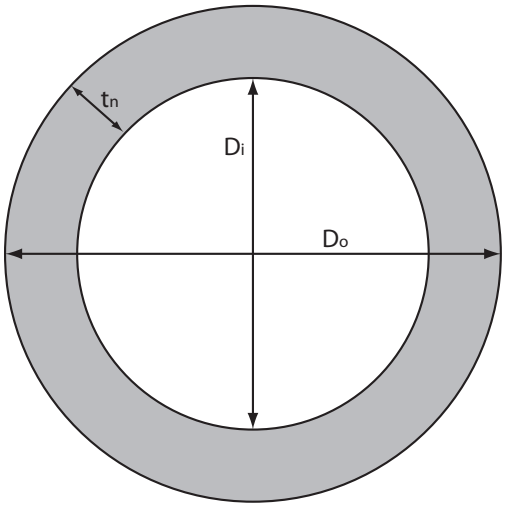

Figure 4.1: Cross-sectional view defining the D/t ratio.

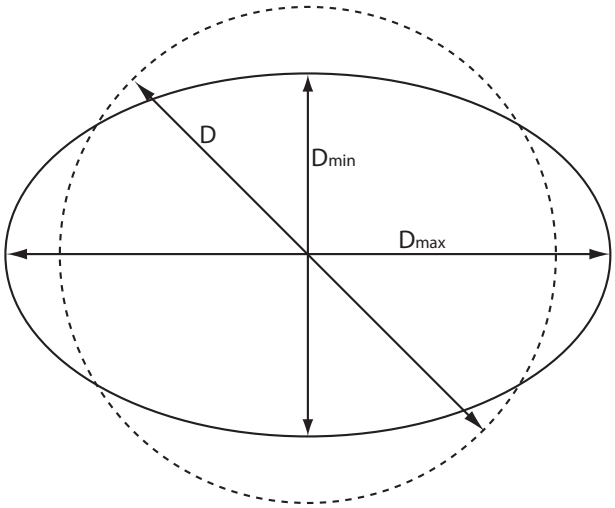

Figure 4.2: Cross-sectional view defining the ovality.

4.4 Fabrication Factor

The fabrication factor is a constant employed to regulate the predicted collapse presssure based on the production technique.

The maximum fabrication factor, α_{fab}, is governed by table 4.1.

Pipe	Seamless	UO	UOE
α_{fab}	1.00	0.93	0.85

Table 4.1: Fabrication Factor for different production methods

The fabrication factor is used to average out the effects of the manufacturing process. Imperfections in the numerical model must account for this constant.

4.5 Collapse Equations

Familiarisation with the governing analytical equations are necessary in order to verify numerical solutions.

The elastic collapse pressure is given in equation 4.3. The structure is assumed to buckle in uniform modes. The derivation is based on non-linear, small strain and moderate rotation kinematics[7]. A linearised eigenvalue buckling matrix is assembled to then yield a solution. This collapse formulation assumes that the pipe is able to sustain deformations upto the onset of collapse while the material is still only experiencing elastic strains.

$$p_{el} = \frac{2E\left(\frac{t}{D_o}\right)^3}{1-\nu^2} \tag{4.3}$$

The plastic collapse pressure is given in equation 4.4. This collapse formulation assumes that the pipe is not able to deform elastically upto the collapse pressure. Plastic strains are induced in order to reach the desired level of deformation.

$$p_{pl} = \sigma_y \alpha_{fab} \frac{2t}{D_o} \tag{4.4}$$

The DNV recommended equation is given in equation 4.5.

$$(p_c - p_{el})\left(p_c^2 - p_{pl}^2\right) = p_c p_{el} p_{pl} f_0 \frac{D_o}{t} \tag{4.5}$$

The Timoshenko equation is given in equation 4.6.

$$(p_c - p_{el})(p_c - p_{pl}) = 3p_c p_{el} f_0 \frac{D_o}{t} \tag{4.6}$$

The Shell equation is given in equation 4.7.

$$p_c = \frac{p_{pl} p_{el} g}{\sqrt{p_{el}^2 + p_{pl}}} \tag{4.7}$$

where

$$g = \frac{\sqrt{1 + p^2}}{\sqrt{p^2 + f^{-2}}}$$

$$p = \frac{p_{pl}}{p_{el}}$$

$$f = \frac{1}{\sqrt{1 + (f_0 D_o/t)^2}} - f_0 \frac{D_o}{t}$$

It is important to note that all collapse pressures are a function of the wall thickness t.

These analytical equations are plotted using MATLAB while varying key parameters. When considering a parameter for variation, other parameters are kept constant at nominal values.

Figure 4.3 shows that the Timoshenko equation is the most conservative. The DNV equation and the Shell equation are relatively close to each other. Clearly the D/t ratio is is highly influencial on the collapse pressure. For lower D/t ratios the pipe collapses plastically and for higher D/t ratios the pipe collapses elastically. The transition ratio, D/t_{tr}, between elastic and inelastic collapse can be determined using equation 6.1. It is important to note that the transition ratio is dependant on the ratio of E/σ_y. The Young's modulus is purely material dependant but if the yield stress is used as a varying parameter, this will change the transition ratio.

$$D/t_t r = \sqrt{\frac{E}{(1 - \nu^2)\sigma_y}} \tag{4.8}$$

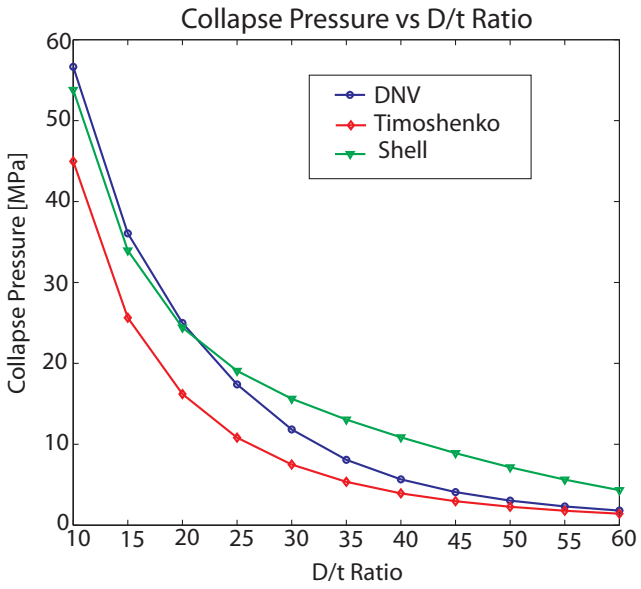

Figure 4.3: Collapse Pressure vs D/t ratio.

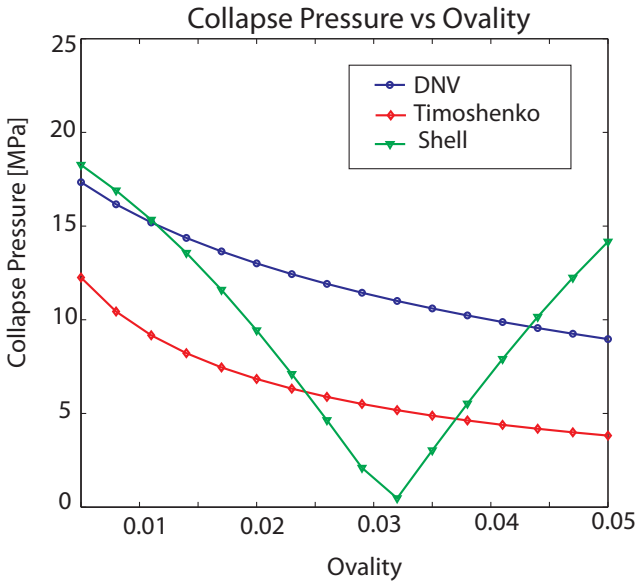

Figure 4.4: Collapse Pressure vs Ovality

Figure 4.4 shows that the collapse pressure is relatively dependant on the

ovality of the pipe's cross-section. The Shell equation experiences a dip in the collapse pressure at $f_o \approx 0.03$. This dip is most likely due to a singular point for the Shell equation and further discussion of this is irrelevant.

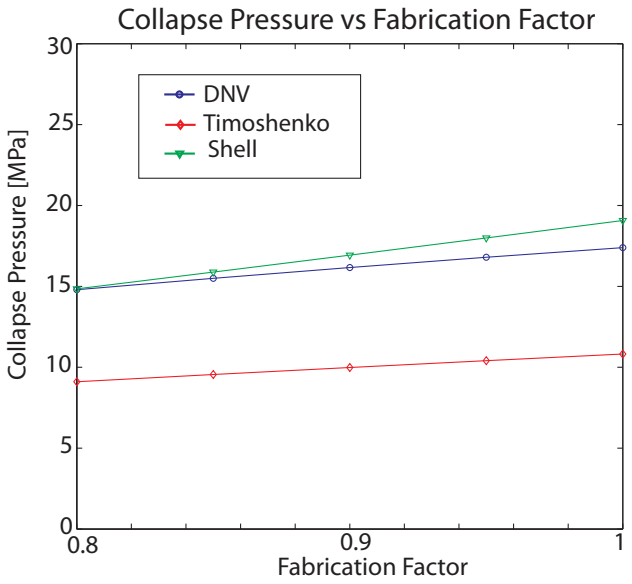

Figure 4.5: Collapse Pressure vs Fabrication Factor

Figure 4.5 shows that the collapse pressure is only marginally influenced by the choice of fabrication factor. Once again the Timoshenko solution is the most conservative while the DNV and Shell equations yield very similar collapse pressures.

Figure 4.6 shows that the yield stress of the material has a strong relation to the collapse capacity. The Shell equation is highly dependant on the yield stress while the Timoshenko is also conservative in its correlation to the yield stress. The DNV equation provides a good compromise between the two extreme cases.

This shows that the DNV equation presents a suitable benchmark for verification of the numerical scheme and sensitivity studies.

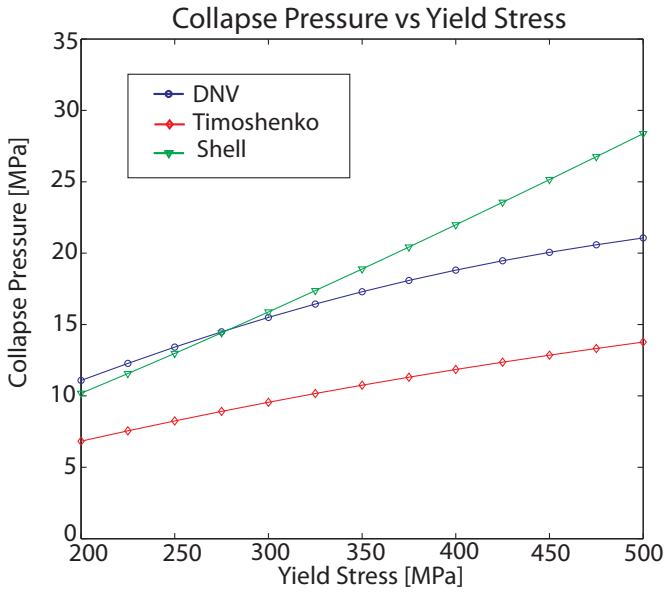

Figure 4.6: Collapse Pressure vs Yield Stress

4.6 Hydrostatic Pressure

It is necessary to consider the nature of hydrostatic pressure which is an essential part of this thesis. One of the key features of a fluid is that it is only able to exert pressure normal to a contact surface. This means that the loading cannot generate shear loads on any surface. The normal pressure loading will always be acting normal to the structure, implying the need for non-linear geometry. This pressure is due to the force of gravity acting upon the fluid that in turn exerts a normally directed pressure on the submerged object.

Consider an infinitesmal cube, shown in figure 4.7, with dimensions dx, dy and dz where z is the direction synonimous with the depth of submersion and taken as positive. The cube is assumed to be in a state of equilibrium.

The pressure acting upon this cube can be expressed as shown in equation 4.9.

$$\sigma_{hyd}(z) = \frac{1}{A}\int_{z_0}^{z} dz \int\int_{A} dxdy\rho(z)g(z) \tag{4.9}$$

Since the object is in equilibrium, only the weight of the fluid column acting

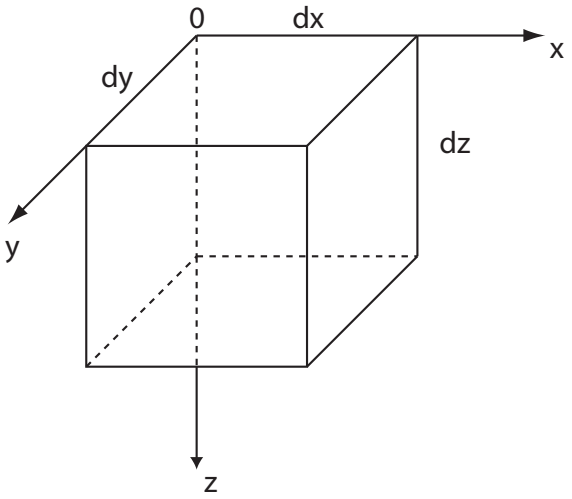

Figure 4.7: Infinitesimal Cube.

from above, z direction, needs to be considered.

$$\frac{1}{A}\int\int_A dxdy = 1$$

Therefore equation 4.9 simplifies to equation 4.10

$$\sigma_{hyd}(z) = \int_{z_0}^{z} dz\rho(z)g(z) \tag{4.10}$$

This now suggests that it is only the depth of submersion, $z - z_0$, that the hydrpstatic pressure is dependant on.

Expression given in equation 4.10 can be simplified based on the following assumptions.

- The fluid is incompressible which indicates that there is no variation of the density throughout the fluid,$\rho(z) = \rho$.
- Variations of the gravitational constant can be negelected as the depth of submersion is much smaller than the radius of earth, $g(z) = g$.

Equation 4.10 can now be simplified to give equation 4.11

$$\sigma_{hyd} = \rho g h + p_{atm} \tag{4.11}$$

Atmospheric sea level pressure, p_{atm}, can be taken as approximately $100kPa$. Conversion to the native units scheme yields, $p_{atm} \approx 0.1MPa$. The density of seawater, ρ, is slightly larger than that of water due to its salt content. Seawater density is approximately $1030kg/m^3$ and after conversion to the native units scheme, $\rho \approx 1 \times 10^{-6} kg/mm^3$. The gravitational constant, g, is known to be $9.81N/kg$and its value is unchanged for the native units scheme. However it would be easier to approximate it as $g \approx 10$. This will help compensate for the rounding down errors of the seawater density.

Looking at a worked example of a depth of 1000 meters in the native unit scheme.

$$\sigma_{hyd} = [(1 \times 10^{-6})(10)(1000 \times 10^3)] + 0.1$$

$$\sigma_{hyd} = (10 + 0.1)MPa$$

It is now evident that the contribution to the hydrostatic pressure from the atmospheric pressure is negligible.

A new simplified formula can now be stipulated to find the hydrostatic stress at a particular depth give in equation 4.12 where h is measured in meters.

$$\sigma_{hyd} = 0.01h \tag{4.12}$$

This will be the basis for relating the pressure loading to the depth of water that the pipe segment is submersed in.

4.7 End Cap Considerations

Full scale collapse tests are performed first by placing the pipe segement to be tested within the test chamber. The test chamber is able to generate the positive pressure in order to simulate hydrostatic pressure. The ends of the pipe are sealed with end caps so that the pressure within the pipe segment will retain atmospheric pressure. The pressure is then permitted to build up within the test chamber, but this now means that the end caps are also being loaded with the hydrostatic pressure. A lateral bar supporting the

two end caps from within the pipe segment can be used so that the pressure that builds up on the end caps is not transfered axially through the pipe but rather through the lateral bar. Figure 4.8 depicts the testing methodology with and without the lateral bar.

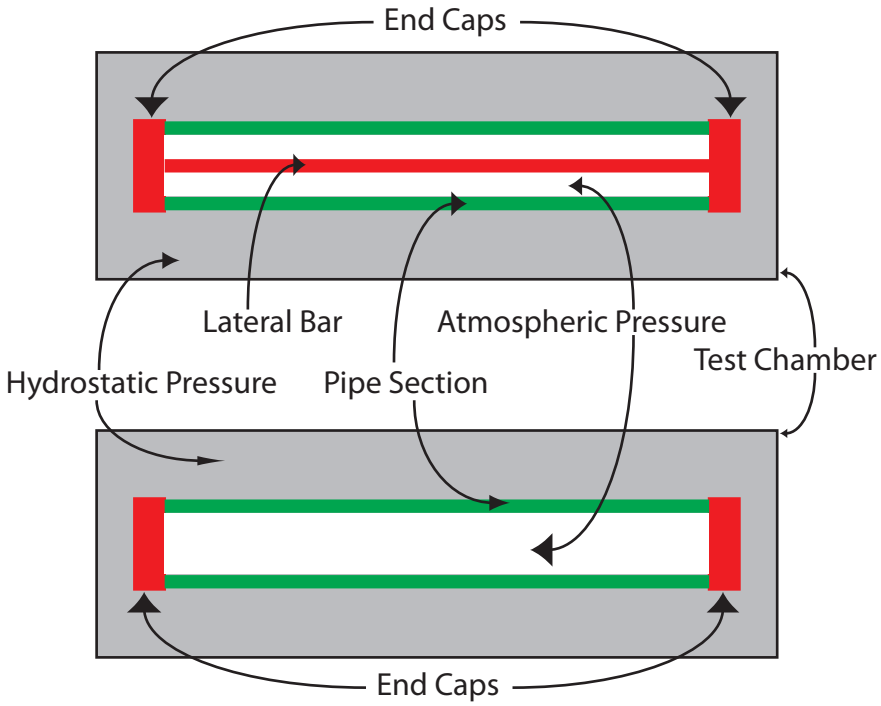

Figure 4.8: Testing Setup

In the abscence of the lateral bar, the area over which the pressure is applied to the end caps is different that the cross-sectional area of the pipe segment. This discrepancy can be resolved by determining the effective force that the end caps transmit to the cross-section of the pipe segment. The effective force will be used in the numerical analysis to simulate the testing procedure when the bar is absent.

Real life testing of pipe segments have end caps on each end such that the hydrostatic pressure that develops over the whole cross section of the pipe is preserved and is transfered to the wall thickness. In order to simulate this loading in ABAQUS, one must account for the area reduction when loading the actual pipe cross section as opposed to loading the whole cross section with an end cap.

Figure 4.9 depicts the necessary parameters to find the effective axial force.

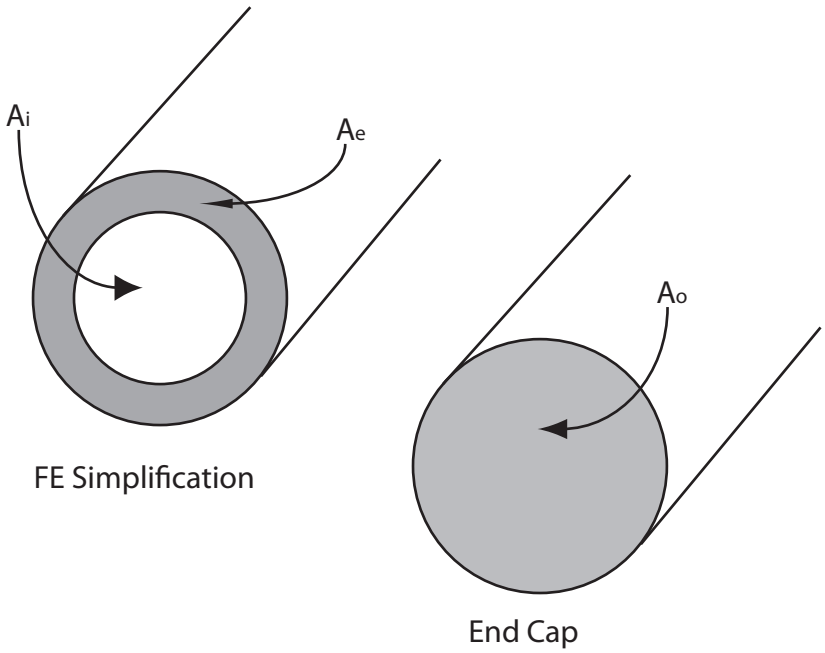

Figure 4.9: Defintion of cross-sectional areas

The area of an ellipse is defined as given in equation 4.13

$$A_{ellipse} = \pi ab \tag{4.13}$$

Where a is defined as the semimajor axis and b is defined as the semiminor axis. The ovality f_0 has been defined in section **??** but needs to be extended to account for the ovality being a scaling factor. These scaling factors are termed β_{max} and β_{min} and are essentially the scaling factors needed to transform the circular cross section of the pipe to an elliptical one. Equations 4.14 and 4.15 define the scaling factors in relation to a and b.

$$a = R\beta_{max} \tag{4.14}$$

$$b = R\beta_{min} \tag{4.15}$$

The updated expression for the area is then given in equation 4.16.

$$A_{ellipse} = \pi R^2 \beta_{max} \beta_{min} \tag{4.16}$$

The outer, inner and effective cross sectional areas are given in equations 4.17,4.18 and 4.19.

$$A_o = \pi R_o^2 \beta_{max} \beta_{min} \tag{4.17}$$

$$A_i = \pi R_i^2 \beta_{max} \beta_{min} \tag{4.18}$$

$$A_e = A_o - A_i \tag{4.19}$$

Applying conservation of forces we can express equilibrium in equation 4.20. The left side of equation 4.20 is for the case when there are end caps during the hydrostatic loading and the right side is in the absence of end caps.

$$P_{hyd} A_o = P_e A_e \tag{4.20}$$

$$P_e = \frac{A_o}{A_e} P_{hyd} \tag{4.21}$$

The final expression is then given in equation 4.21. This expression will be implemented into the numerical in order to simulate the end cap loading in the abscence of the lateral bar shown in figure 4.8.

4.8 Residual Stresses

The cold forming process involved in the UOE forming process often induce residual stress fields. In particular the circumferential residual stress is the most influential for the collapse pressure[7].

The process of bending a plate to a tubular is a symmetrical process so only half of the cross-section needs to be considered. This is depicted in figure 4.10 with point 1 representing the undeformed state, and point 5 representing the completely deformed semi-circle. This simplification does not account for the contraction and expansions stages but simply the major contribution from

pure bending. In order words, the axial, with respect to the beam, or the circumferential, with respect to the semi-circle, will exhibit maximum stress magnitudes on the top and bottom surfaces and zero stress along the neutral axis. The internal face of the semi-circle will be in compression and the exterior face will be in tension.

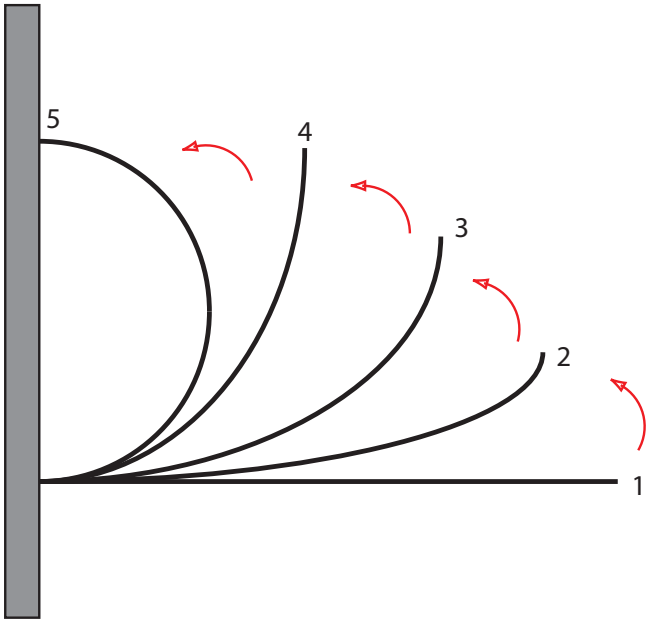

Figure 4.10: Pure bending of a beam to a semi-circle

In order to measure the amount of circumferential residual stress stored, a section of the pipe specimen is removed. The resulting ring is then split axially, allowing the ring to either open or close. The amount by which the ring opens or closes is used to find the specimens circumferential stress. If the ring opens, this indicates that internal face is in compression and the external face is in tension, and if the ring closes, the opposite is true.

Figure 4.11 depicts a ring splitting test resulting in an opening. The expression for the maximum magnitude of circumferential stress, which is based on thin-walled theory, is presented in equation 4.22[7].

$$|\sigma_{res}| = \frac{Et}{4\pi R}\alpha \tag{4.22}$$

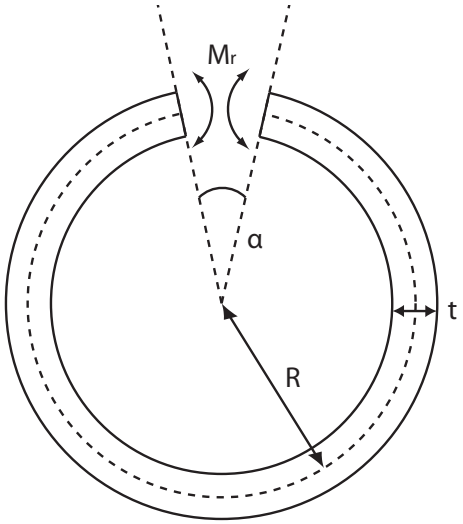

Figure 4.11: Ring splitting residual stress determination.

Upon examining the stress distributions of a beam subject to pure bending, the necessary insight has been generated to implement these residual stresses in the numerical analysis.

4.9 Material Models

In order to perform a fully non-linear analysis, material models need to be incorporated to mimic the true behaviour of steel. This section will serve as a reference for the implementation of non-linear material properties into the numerical simulation.

Linearly Elastic Material Model

This model is defined by the materials Young's modulus, E. A perfectly elastic material model indicates that the stresses and strains of the material are proportional for all stresses and strains up to fracture. This is a poor model to represent the complete material response of steel. It is however always present in every material model and valid for a limit magnitude of strains.

Figure 4.12 shows the material properties for a perfectly linear elastic distri-

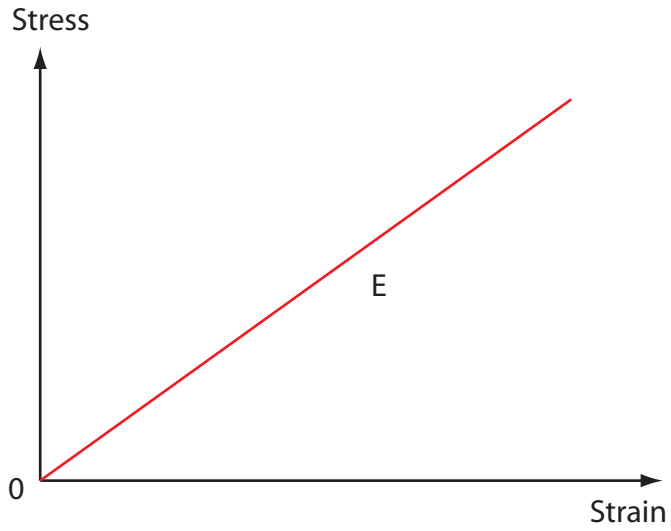

Figure 4.12: Stress-strain curve for a linearly elastic material.

bution. The Youngs modulus is defined as the gradient along the stress-strain curve. Equation 4.23 shows this relation.

$$E = \frac{\sigma}{\varepsilon} \tag{4.23}$$

Allowing the material properties to vary in a non-linear manner is a relatively simple implementation in a FE package. There are several non-linear material models available with varying degrees of accuracy and simplicity can be used to model the exact material properties.

Perfectly Plastic

This model is defined by E and the yield stress, σ_y. At a specified yield stress, the material displays complete plastic behaviour. This is a relatively simple model but in some cases provides and excellent representation of the material properties, allowing the results to be a lower bound in comparison to other material models.

Figure 4.13 shows the material properties for a perfectly plastic material model. The material behaves elastically up to the yield stress, at which point it displays purely plastic behaviour.

Hardening Model

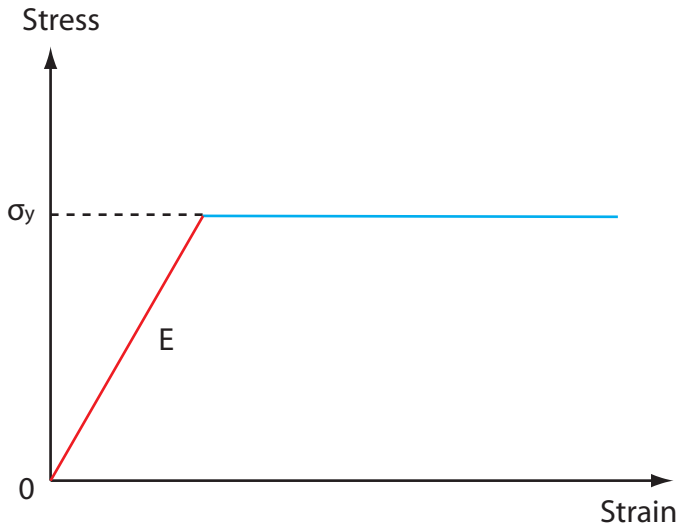

Figure 4.13: Stress-strain curve for a perfectly plastic material.

This model is defined by E, σ_y and the hardening modulus, H. The material behaves linearly elastic upto the yield stress, at which point instead of permiting perfectly plastic behaviour, the material allows for a certain amount of strain hardening. The degree of strain hardening is governed by the materials hardening modulus, usually defined as a fraction of the materials Young's modulus. This model allows for the structure to store a greater amount of strain energy than compared with the perfectly plastic model.

Figure 4.14 shows the material properties for a hardening material model which may also be referred to as bi-linear hardening model.

Luder Plateau

This model is defined by E, σ_y, H and the Luder plateau strain, ε_{lp}. It is essentially the hardening model however after the yield point, instead of exhibiting linear hardening immediately, there is a small degree of perfect plasticity before the onset of the hardening behaviour.

Figure 4.15 shows the material properties for a hardening material with the Luder plateau depicted with a green line.

Ramberg-Osgood

The Ramberg-Osgood material model is based on the power series. Choosing the right fitting parameters can allow extreme consistency with experimental

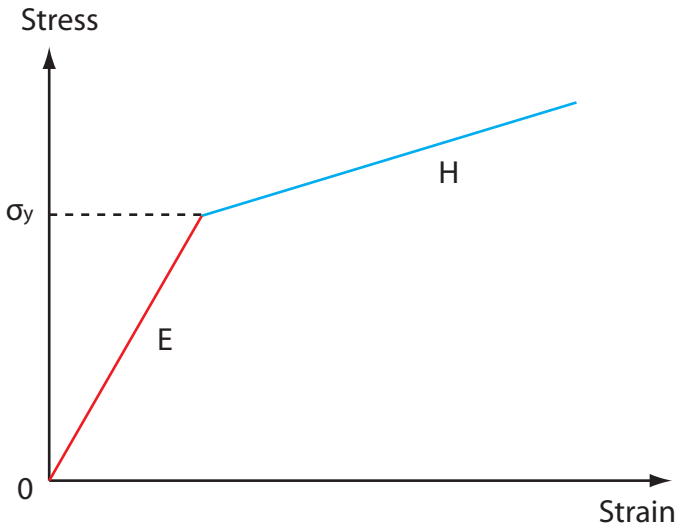

Figure 4.14: Stress-strain curve for a hardening material model.

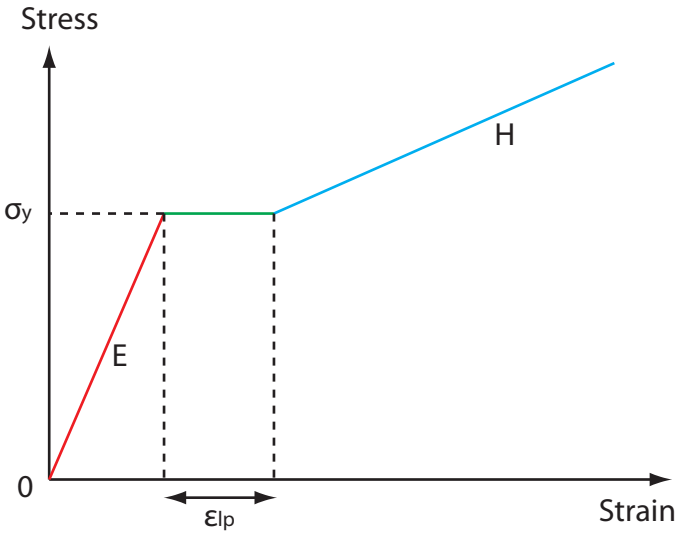

Figure 4.15: Stress-strain curve for a hardening material model with a Luder plateau.

material data[7]. The expression is given in equation 4.24.

$$\varepsilon = \frac{\sigma}{E}\left[1 + \frac{3}{7}\left(\frac{\sigma}{\sigma_y}\right)^{n-1}\right] \tag{4.24}$$

where E, σ_y and n are predefined fit parameters.

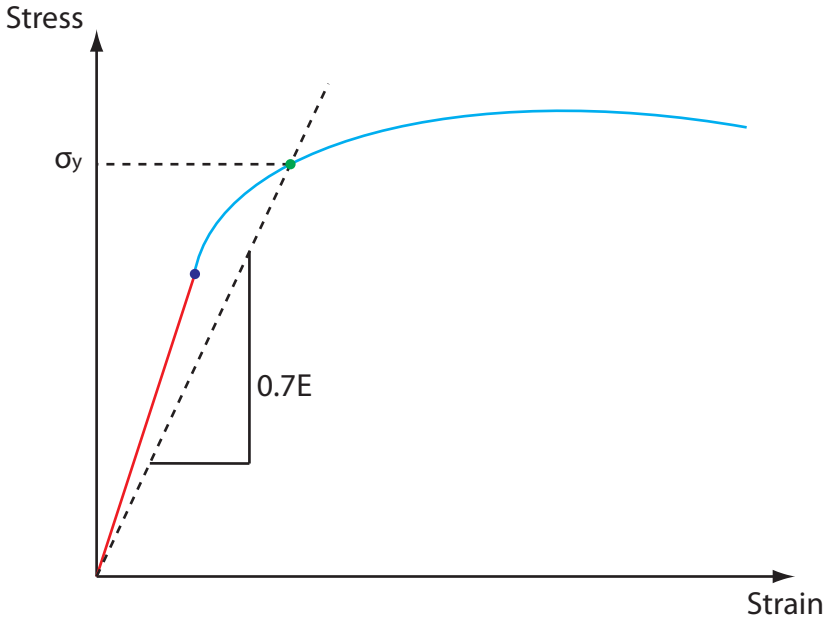

Figure 4.16: Stress-strain curve for a Ramberg-Osgood material model.

Figure 4.16 gives a visual representation of how the fit parameters interact.

- E is the slope of the linearly elastic part of the curve depicted with a red line.
- σ_y is the intersection of the dotted line from the origin with a gradient of $0.7E$.
- n can be found from measured stress-strain data. It essentially controls the shape of the curve during the strain hardening phase.

The Ramberg-Osgood function is programmed into MATLAB to exemplify the effect of the fit parameters. Using the parameter values, $E = 200$ GPa and $\sigma_y = 500$ MPa. Plotting this function for 3 cases of n is shown in figure 4.17.

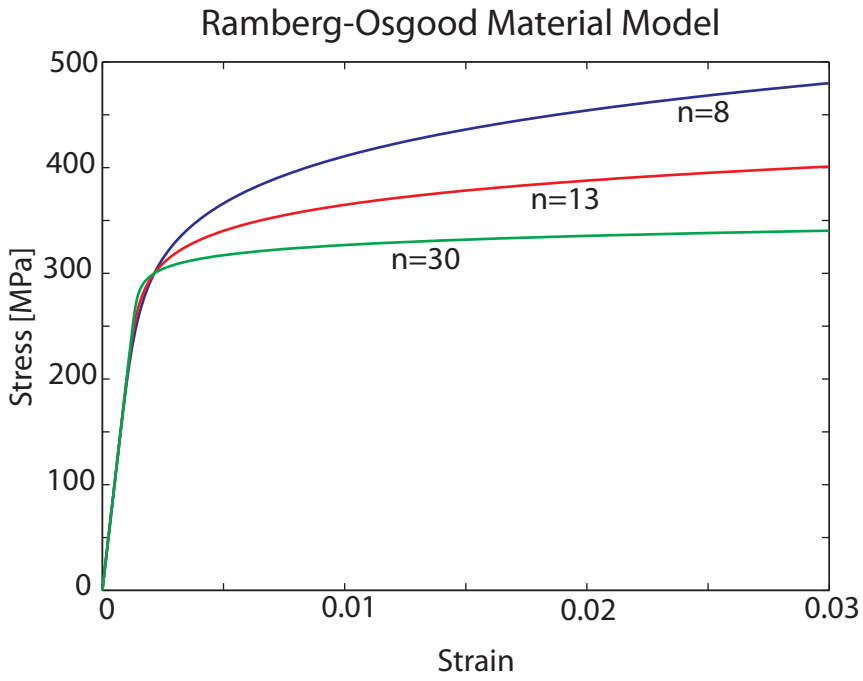

Figure 4.17: Stress-strain curve for a Ramberg-Osgood material model with various values of n.

The fitting parameter n is clearly an indicator of how plastic the materials behaviour is beyond the yield stress. The post yield stress distribution when $n = 8$ shows a relatively high hardening modulus compared to the other two cases. The post yield distribution when $n = 30$ shows an extremely low hardening modulus, almost perfectly plastic in behaviour. This gives a clear picture of the stress-strain behaviour correlating to the choice of n. The Ramberg-Osgood model has the advantage that the onset of plasticity is not sudden as with the previous models. The gradual response from elastic to plastic will give a better representation of the true material properties.

The Bauschinger effect can be observed during the cold expansion stage of the UOE production process. During the expansion stage, the pipe builds up tensile hoop stresses with results in a reduced compressive yield strength. It is however possible to preserve the compressive strength by mild heat treatment as discussed in[13], [14], [15]. This means that applying anisotropic material properties is redundant so long as mild heat treatment is applied to help

recover the compressive yield strength. Isotropic material properties will be assumed.

4.10 Riks Method

Structural problems involving unstable and geometrically non linear collapse, require an alternative numerical method to account for inelastic effects. Linearised eigenvalue analysis bases itself upon small deformation theory and requires material properties to be defined in a linear manner. The Riks method provides an iterative scheme that can account for a response that is highly dependant on the loading path in the load-displacement space..

The Riks method bases itself upon the Newton-Rhapson method, which is a numerical scheme used primitively to find intersections but can naturally be applied to finding the equilibrium point along the load-displacement path. The numerical scheme that ABAQUS implements can be found in [4], but the main points will be covered for completeness.

Application of the Riks method requires that that the loading is governed by a single scalar [2]. The loading is going to simulate hydrostatic pressure loading, which has been shown in section 4.6 to be only dependant on the depth of submersion. The Riks method also requires the loading to be proportional, which again agrees with this loading pattern.

The Riks method needs to be the last step in the FE simulation and any loads that are to be constant during the Riks analysis must be declared prior to the Riks step which will then be treated as a dead load. The loading function is given in equation 4.25.

$$P_{tot} = P_{dead} + \lambda(P_{ref} - P_{dead}) \tag{4.25}$$

In order to acheive the desired collapse mode, the FE model must include imprefections that encourages the structure to collapse in the desired mode. This is to ensure that there is some response in the particular buckling mode before the critical load is reached. There are several parameters than can be specified to controls the schemes behaviour. Most of these parameters are internally optimsed by ABAQUS but there are however 3 important termination criteriums.

1. Node number for monitoring displacement, N_{mon}.

2. The degree of freedom related to N_{mon}, denoted DOF_{mon}.

3. The magnitude of displacement for N_{mon}, denoted v_{mon}.

The criteria for termination of the Riks method is important as it helps to end the simulation after the maximum load has been acheived. This saves unnecessary processing time in the post buckling region of the pipes response.

The monitor node, N_{mon}, and DOF_{mon} is selected based on the expected collapse shape which is usually determined by the direction of ovality. The mangnitude of displacement, v_{mon}, is simply set to 25% of the cross-sections inner radius which ensures that the maximum load has been acheived. This also allows the contact condition to be removed as the interior surfaces will never contact each other.

Chapter 5

Finite Element Approach

5.1 Implementation

The finite element package ABAQUS Standard(V6.9) is used to perform the numerical analysis.

After considering the nature of the problem the following parameters have been chosen for implementation into the numerical scheme.

- Initial residual stresses, σ_θ
- Geometric imperfections
- Material models
- Loading conditions
- Boundary conditions

Figure 5.1 depicts the conceptual design behind the FE implementation.

5.2 Monolithic Pipe

A complete analysis of the purely monolithic pipe has been previously done[11]. Similar imperfections and modelling methodology was used generate the

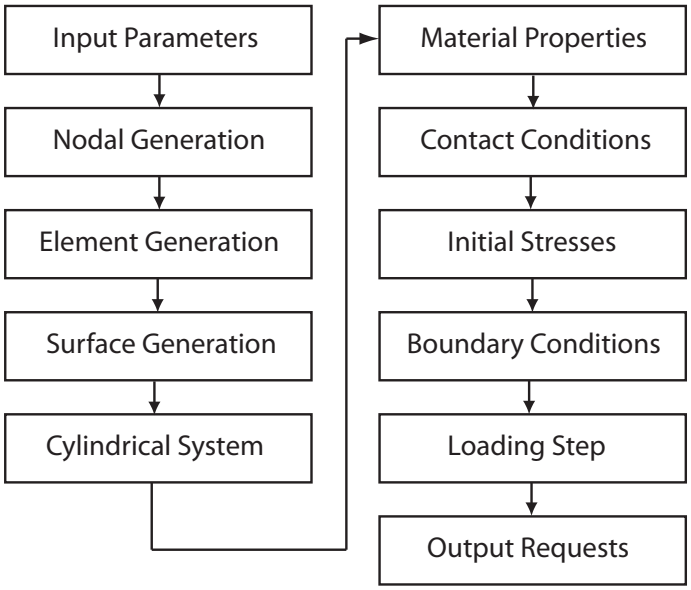

Figure 5.1: Flow chart of the input file.

cladded pipe model, but a completely independant input model was created. The previous work served as a reference point to verify the monolithic and cladded pipe simulations.

5.3 Model Generation

All variable parameters of the problem need to be declared at this stage. Certain parameters have been previously introduced.

The length of the pipe, L, is defined using a pipe length factor, L_p. Equation 5.1 shows their relationship.

$$L = L_p D_o \tag{5.1}$$

In order to ovalise a circular cross-section, a scaling factor must be applied along the major and minor axis. Equations 5.2 and 5.3 show the correlation.

$$\beta_{max} = 1 + \frac{f_0}{2} \tag{5.2}$$

$$\beta_{min} = 1 - \frac{f_0}{2} \tag{5.3}$$

Inner and outer areas of the cross-section is calculated in order to determine the correct end cap forces to be applied as presented in section4.7. Declaring all the nodes for the model require that the key nodes are declared in a cylindrical coordinate system after which the nodes are generated using nodal functions.

Nodal numbering consists of 8 digits. The first digit is used a special digit. A 0 indicates the node is part of the main model. An 8 indicates that the node is part of the CRA section of the pipe. The seam weld of the pipe is treated with a seperate generation procedure so that local imperfection can be implemented. The second two digits represent the axial position of the node while the next two digits represent the radial position. The last three digits represent the circumferential position of the node shown in figure 5.2.

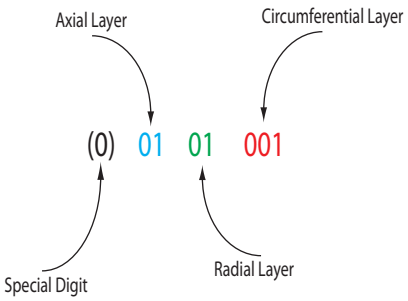

Figure 5.2: Nodal Numbering Scheme.

Nodal sets are created for the front and back cross-sections of the pipe so that boundary conditions can be applied. The choice of element type was primarily between shell or continuum elements. The wall thickness of the pipe section can quite large indicating that transverse shear deformations can be an influential factor. Being prepared for unexpected behaviour meant choosing continuum elements which ensure that all stresses and strains will be available. Accordance with the element choice of previous work enforces

the use of continuum elements. An 8 node, three-dimensional element with reduced integration is used. Reduced integration allows for faster processing times and a softer model[12]. The element numbering scheme is identical to nodal numbering scheme depicted in figure 5.2. All elements have to be placed into sets by their radial position in order to allow for the circumferential residual stresses to be specified.

Surface generation is a performed so that surface-based loading can be applied during the analysis step. The interior surface of the pipe is generated so that contact conditions can be formulated while the exterior surface is generated so that hydrostatic loading can be applied. The front and back cross-sectional surfaces are defined so that end cap loading can be applied if necessary.

A cylindrical coordinate system is the natural choice with the pipe segments axial direction alligned with the z axis. Boundary and coupling conditions can be specified easily and all output requests will be given in the cylindircal system. Material properties of the backing steel and cladding need to be assigned. Material properties are applied isotropically using true strains and stresses. Contact conditions are applied to the inner surface in the event that the loading continues until the interior walls make contact with each other. The contact condition results in increased processing time so is ommited from the simulation as the contact part of the analysis is already beyond the point of interest.

The wall thickness variation can be represented by a diemnsionless quantity called the eccentricity which is calculated using equation 5.4.

$$ec = \frac{t_{max} - t_{min}}{t_n} \tag{5.4}$$

Eccentricity can manifest locally or globally. Figure 5.3 shows the global wall thickness variation and the eccentricity, ec, defined also by the vertical distance between the centers of the two circles.

Figure 5.4 shows the local wall thickness variation. In this case there is a wall thickness reduction but can also manifest as a wall thickness increment. The parameter, β_{inf}, defines the angle of influence of the local wall thickness variation. The local wall thickness variation is to simulate the prescence of the seam weld characteristic of UOE produced pipe sections. The angle of influence is choosen to be $\beta_{inf} = 8$ degrees.

The seam weld on UOE produced pipes may not just exhibit wall thickness

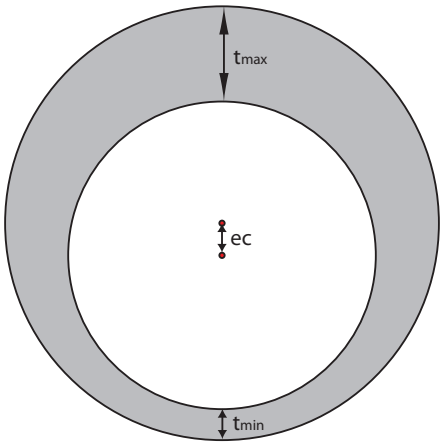

Figure 5.3: Cross-sectional view defining global wall thickness variation.

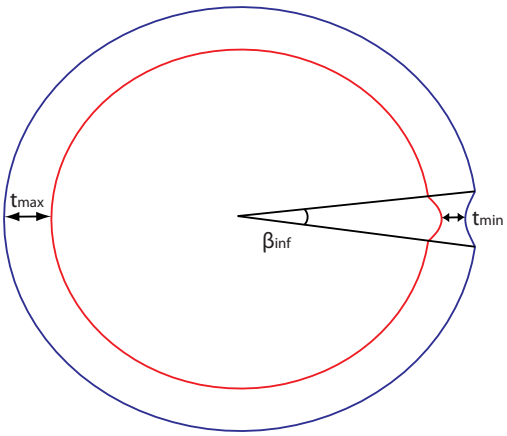

Figure 5.4: Cross-sectional view defining local wall thickness variation.

variations. Peaking and flattening of this seam welded area may also be natural imperfections that need to be implemented. These relate to the cross-sections ovality defined in equation 4.2. Peaking of the seam weld is shown in figure 5.6.

This will allow the numerical model to mimic the characteristics of a seam

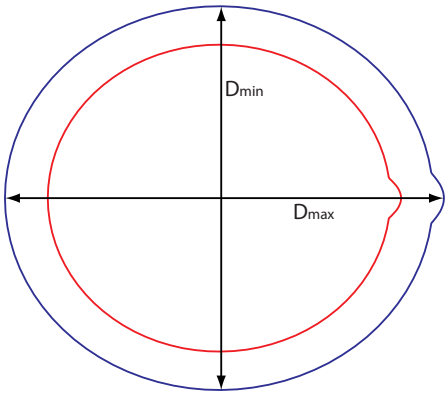

Figure 5.5: Cross-sectional view defining peaking.

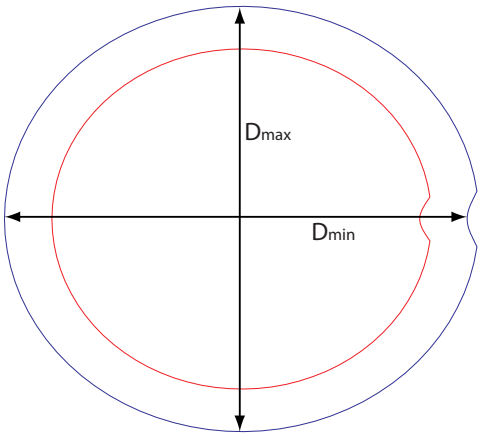

Figure 5.6: Cross-sectional view defining flatening.

welded pipe. The actual values choosen for geometric imperfections are enforced to account the constant, α_{fab}, in the FE scheme. The verification process will help determine the ideal values for imperfections based on full scale results.

The inner cladding will be perfectly alligned with the geometrically imperfect

backing steel. This means that the cladding layer will essentially inherit the geometric imperfections imposed on the backing steel.

5.4 Boundary Conditions

The boundary conditions that are applied to the FE simulation are symmetrical. Therefore only one half of the pipe section is actually modelled in order to reduced processing time by half. One end of the pipes cross-section receives a z-symmetrical boundary conditions as shown in figure 5.7. The other end of the pipes nodes need to be coupled to the center point of the cross-section shown in figure 5.7. The other end of the pipe specifyies the nodal boundary conditions for a single central point, all points of the cross-section will follow the restrictions placed on the central node.

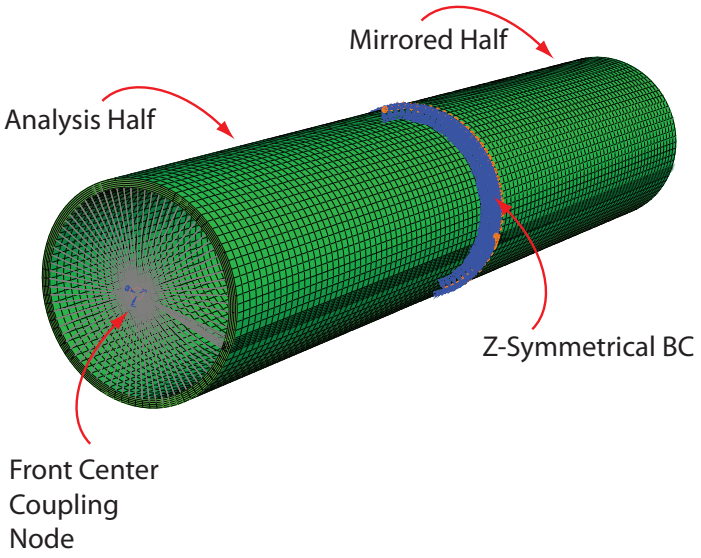

Figure 5.7: Boundary Conditions and Coupling Constraints.

In order to generate appropriate boundary conditions, attention has to paid to the degrees of freedom that the front central node is permitted, and also which degrees of freedom should be coupled to this node. A summary over the different boundary conditions is given in table 5.1.

Type	Center Node Constraint DOF	Constraint Coord Sys	Coupling DOF	Coupling Coord Sys
Capped End	1,2,4,5,6	Global	1,2,3,4,5,6	Cylindrical
Clamped End	1,2,3,4,5,6	Global	1,2,3,4,5,6	Cylindrical
Infinte Pipeline	1,2,4,5,6	Global	2,3,4,5,6	Cylindrical
Plane Strain	1,2,3,4,5,6	Global	2,3,4,5,6	Cylindrical
Plane Stress	1,2,4,5,6	Global	2,4,5,6	Cylindrical

Table 5.1: Boundary Conditions and Coupling Constraints

5.5 Initial Stresses

The geometry of the model allows multiple elements in the radial direction of the pipe. Considering the discussions in section 4.8, a maximum residual stress is declared which then distributes itself over the cross-section.

Considering this in a FE perspective, the inner radial layer will have the greatest value of residual stress, and the outer radial layer will have the lowest value. The maximum value can be calculated using equation 4.22. ABAQUS will resdistribute these initial stresses which is dependant on the geometric imperfections. The redistribution prior to hydrostatic loading is shown in figure 5.8. The actual residual stresses that reside in each layer of the FE model can be read from circumferential stress output requests.

5.6 Loading

Hydrostatic loading has been considered in section 4.6 and the option of loading the end caps have been considered in section 4.7. The magnitude of the pressure is increased incrementally through the numerical scheme used to establish equilibrium.

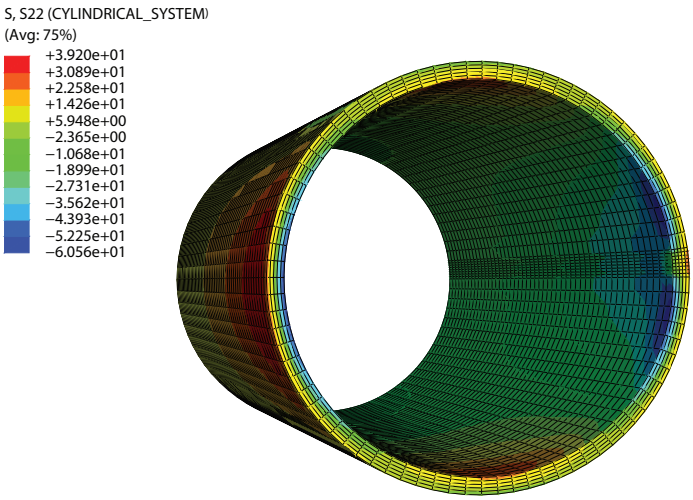

Figure 5.8: Redistribution of circumferential residual stresses.

The first step is a referred to as a Pre-Step where stress and strain requests are made prior to loading the structure. This is primarily to verify how the specified residual stresses redistribute through the model.

5.7 Convergence Analysis

The number of elements used to represent the model needs to be selected carefully. Too many elements will result in excessive processing time, and insufficient elements will yield inaccurate results. The pipe segments mesh is based on the number of radial, circumferential and axial elements. The pipe segment without an inner cladding is considered for the mesh refinement.

A mesh convergence analysis is performed by first choosing a very coarse mesh in all 3 direction and then slowly refining the mesh until mesh increments in any direction will result in a less than 1% deviation in results. The structure will grow softer as the mesh density increases, so the collapse pressure will approach the denser mesh from higher values.

At this stage only global imperfections such as ovality and global thickness variation can be included and activated in the numerical model used for the

mesh refinement. Local peaking and flattening require that the circumferential mesh density be finalised.

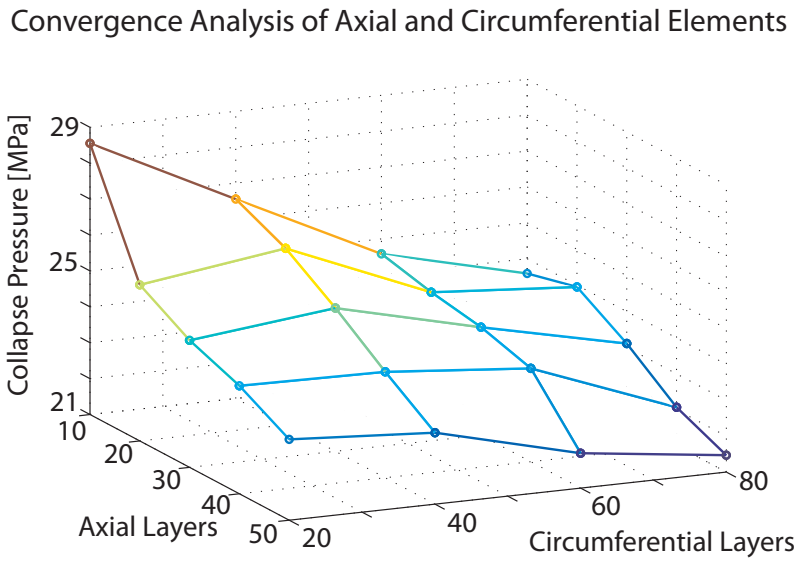

Figure 5.9: Mesh Convergence Analysis for circumferential and axial elements.

Figure 5.9 and figure 5.10 shows the results on the mesh analysis. Convergence was found with 5 radial, 80 circumferential and 50 axial layers. The models mesh size will remain fixed at $20,000$ elements from this point on. ABAQUS's input file syntax lacks logical statements so any imperfections introduced into the model will be based on this mesh size to ensure a working model.

On the basis of the convergence analysis and the geometric similarities between the backing steel and cladding, the same mesh size will be used to represent the cladding material.

5.8 Verification

A fair amount of full scale tests have been performed for which experimental data is available. The experimental data is extracted for relevant cases and

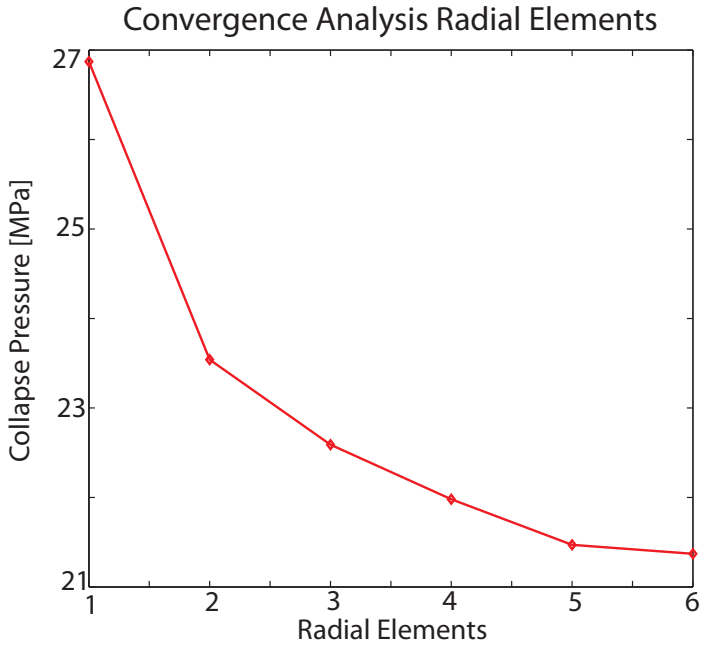

Figure 5.10: Mesh Convergence Analysis for radial elements.

converted to the natuve unit scheme. Analytical and numerical solutions will be calculated in order to verify the integrity of the numerical scheme. Tables 5.2, 5.3 and 5.4 span horizontally giving necessary information to find analytic and FE solutions. Yield stress is determined nominally from sources that give anisotropic material properties. The length factor used in the FE model is chosen as 5 when not specified. A monolithic FE model is used with the recommended mesh density. A perfectly plastic material model was used.

Data Source

- Pipe 1 and 2 found in[17].
- Pipe 3, 4 and 5 found in[19].
- Pipe 6,7 and 8 found in[18].
- Pipe 9, 10 and 11 found in[15].
- Pipe 12, 13 and 14 found in[14].

Pipe	API Grade	D_o(mm)	t(mm)	L_p
1	X65	660.4	25.4	3
2	X65	660.4	25.4	NS
3	X65	509.5	11.55	NS
4	X65	508.0	19.04	NS
5	X65	525.7	23.65	NS
6	X65	353.1	22.07	NS
7	X65	325	18.37	NS
8	X65	323.4	21.17	NS
9	X65	508	28.58	8.8
10	X65	508	28.58	8.8
11	X60	660.4	41.28	13.3
12	NS	457	25.4	12
13	NS	457	25.4	12
14	NS	457	25.4	12
15	X65	609.6	31.8	NS
16	X65	609.6	31.8	NS
17	X65	609.6	31.8	NS

Table 5.2: Full Scale Basic Data

- Pipe 15, 16 and 17 found in[13].

Figure 5.11 shows the collapse pressures for each pipe compared to analytical and numerical solutions.

The FE solution behaves quite well when compared to the DNV analytical solution, yielding slightly higher collapse pressures. The DNV solution is also conservative when compared to the full scale test data. There is quite a large discrepancy between pipes 10 and 13. This is due to the heat treatment these particular pipes have received which helps to restore some of the pipes strength lost during the UOE process. The analytical solution uses the fabrication factor to account for the UOE process, while the FE model applies geometric imperfections and residual stresses. The FE model is responding well to changes in the key parameters such as D/t ratio, ovality, yield stress and residual stresses. The FE scheme is deemed viable for the sensivity analysis.

Pipe	Pipe Condition	End Condition	D/t Ratio	$f_0(\%)$	$ec(\%)$
1	CR	UR	26	0.38	1.2
2	TMCP	NS	26	0.23	0.8
3	NS	ECL	44.1	0.246	NS
4	NS	ECL	26.7	0.108	NS
5	NS	ECL	22.2	0.086	NS
6	NS	NS	16.0	0.39	5.3
7	NS	NS	17.7	0.20	9.7
8	NS	NS	21.17	0.23	6.6
9	TMCP	UR	17.77	0.18	NS
10	HT	UR	17.77	0.17	NS
11	TMCP	UR	16.0	0.23	NS
12	TMCP	UR	18	0.12	NS
13	HT	UR	18	0.125	NS
14	TMCP	UR	18	0.10	NS
15	HT	ECL	19.2	0.428	NS
16	AR	ECL	19.2	0.368	NS
17	AR	ECL	19.2	0.384	NS

Table 5.3: Full Scale Imperfection Data

Pipe	σ_{res}	σ_y	p_{exp}	p_{DNV}	p_{fe}
1	34	350	18.7	18.1157	19.62
2	53	392	19.0	19.3267	20.68
3	NS	476	4.56	4.8072	5.02
4	NS	444	17.6	19.2042	19.98
5	NS	402	23.0	26.2475	28.96
6	37	589	70.3	57.4276	62.15
7	177	536	57.3	46.2944	49.77
8	91	491	63.9	32.8870	36.49
9	NS	500	43.58	43.3156	45.38
10	NS	500	60.94	43.3156	49.49
11	NS	500	49.06	49.3371	48.45
12	24	379	35.8	33.0411	35.05
13	18	482	50.3	41.2246	40.68
14	53	482	41.2	41.2246	39.56
15	NS	565	45.1	42.8699	44.69
16	NS	550	37.2	42.0072	43.50
17	NS	520	37.0	40.2000	42.62

Table 5.4: Full Scale Stress Data (MPa)

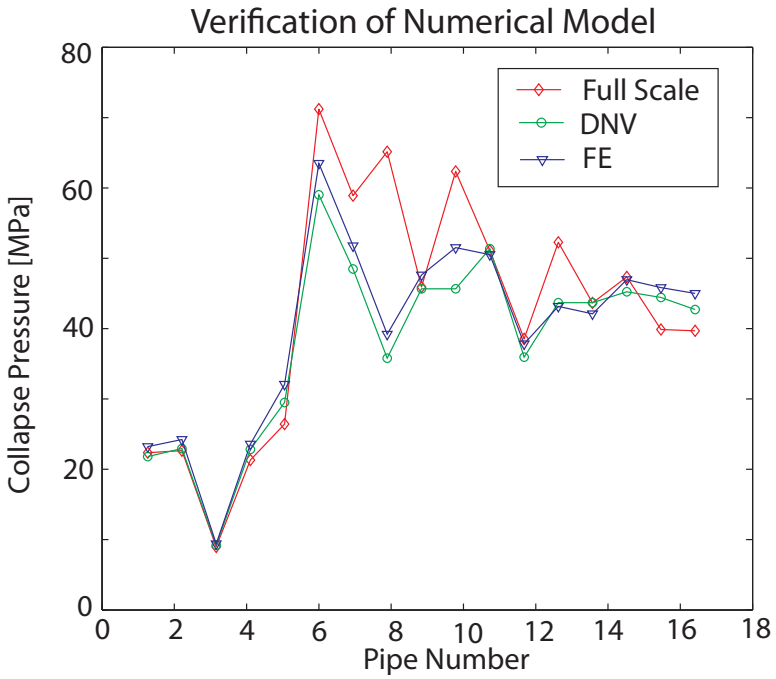

Figure 5.11: Verification of FE solution.

Chapter 6

Sensitivity Study

6.1 Preliminaries

Considering the vast amount of parameters that can be varied in such a problem it is necessary to make certain assumptions. A parameter that is chosen to be varied will be varied as specified, but other parameters remain constant at a median value so as to ensure the particular effect is activated but not dominant.

The inner cladding's thickness does not contribute to the D/t ratio, because current standards do account for the strengthening capability of the cladding. The limit state of the particular application is then determined on the collapse capacity of the backing steel and not the inner cladding.

Flattening and peaking of the modelled seam weld affected the ovality very insignificantly. Initial ovality that manifests in a global manner has a greater influence on the collapse pressure. The flattening and peaking can dominate, but their magnitude then needs to be unrealistically high. Full scale test data suggests that peaking and flattening are minimal, so we can discard this property from the sensitivity study. All ovality will be declared globally to find the lowest collapse pressure.

The eccentricity of the model could also manifest locally or globally. Extreme local thickness variations is deemed irrelevant based on verification data. The eccentricity yielded lower collapse pressures when declared globally.

The material properties of the monolithic numerical solution are fixed as a Ramberg-Osgood material model for $n = 30$. This will ensure that effects

from the backing steel are suppressed.

The initial stresses are applied to the monolithic part of the pipe and then allowed to redistribute the stresses through the whole thickness. Reported initial redistributed stresses are approximately 40% lower than declared for nominal thicknesses.

6.2 Results

The parameter variation is decribed in table 6.1.

Parameter	D/t Ratio	Start	End	Increment
D/t	NA	15	40	2.5
f_0	15,25	0.005	0.05	0.005
ec	15,25	0.1	1	0.1
t_{CRA}	15,25	2	10	1
BC	15,25	1	5	1
L_p	15,25	4	6	0.5
σ_y	15	250	520	30
n	15	8	30	NA
σ_{res}	15,25	0	150	NA

Table 6.1: Sensitivy study

Geometric

The DNV recommended equation is included as a baseline in plots where it gives useful meaning. The term monolithic is synonimous with backing steel.

Figure 6.1 shows the collapse pressure distribution when the D/t ratio is the varying parameter. The monolithic numerical solution is in good accordance with the analytical DNV equation. The cladded solution gives a clear increase in the collapse capacity across the whole D/t range. The strengthening effect is however less pronounced for lower D/t ratios. This is primarily due to the fact that the thickness of the inner cladding is not taken as part of the D/t ratio. The proportion of the wall thickness that consists of the inner cladding is larger for higher values of D/t. The collapse pressure distribution is very smooth for both the monolithic and cladded cases, indicating that the numerical model yields stable solution. All solutions are responding similarly to the variation.

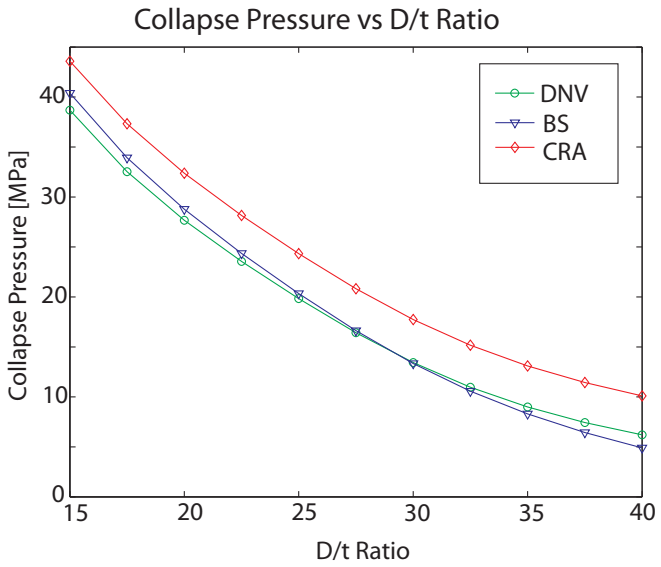

Figure 6.1: Collapse pressure vs D/t ratio for monolithic and cladded pipe

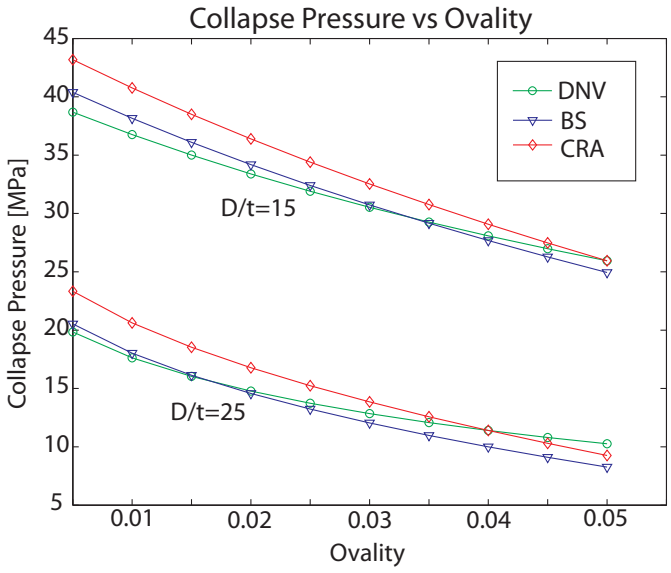

Figure 6.2: Collapse pressure vs ovality for monolithic and cladded pipe

Figure 6.2 shows the collapse pressure distribution when the ovality is the

varying parameter. The DNV baseline is strongly affected by the pipes initial ovality and more responsive for the lower D/t ratio. The monolithic case yields similar values as the DNV baseline. The cladded solution displays increased strength over the entire ovality range, and seems to mirror the monolithic distribution. This indicates that the cladding is strengthening the pipe section but due to the extra wall thickness.

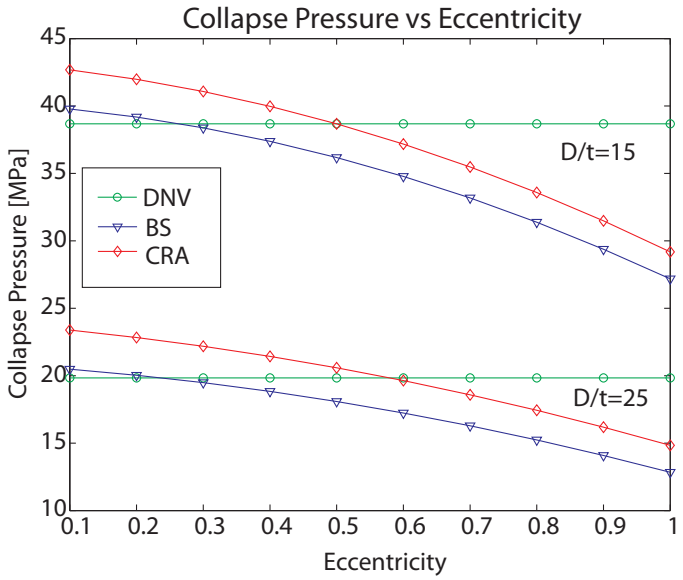

Figure 6.3: Collapse pressure vs eccentricity for monolithic and cladded pipe

Figure 6.3 shows the collapse pressure distribution when the eccentricity is the varying parameter. The DNV solution does not include the eccentricity as part of the equation so is simply a constant value over the distribution. The monolithic solution is quite unresponsive when $ec = 0.1 \rightarrow 0.4$, but beyond this point the collapse pressure begins to fall quite dramatically. The fall in collapse pressure is more pronounced for the lower D/t ratio. Section 5.8 showed that extreme eccentricity as the range depicts in figure 6.3 is unrealistic. The cladded solution displays a strengthening effect over the whole range, and displays a similar response to the monolithic solutions. Again the cladded case is seen to have a greater strengthening effect for the higher D/t ratio.

High values of eccentricity generated an alternative collapse profile depicted in figure 6.4. This indicates that the magnitude of the initial ovality of the pipe segment was insufficient to acheive the desired collapse mode. The

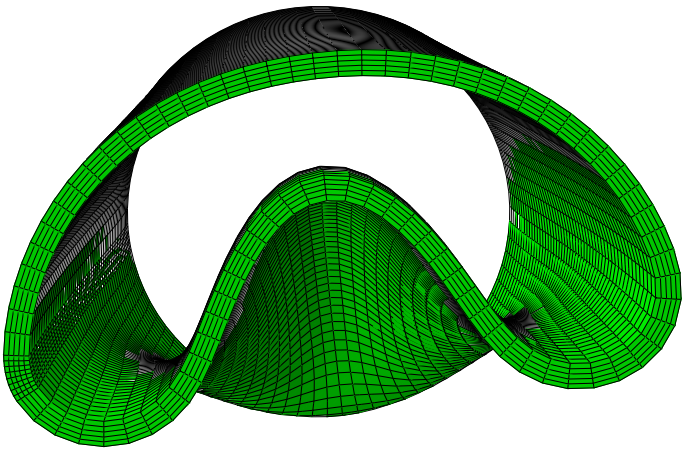

Figure 6.4: Cross-sectional of post collapse form

eccentricity effects have dominated the collapse shape. This is not of importance as this collapse profile is only experienced for unrealistically high values of eccentricity.

Figure 6.5 shows the collapse pressure distribution when the cladding thickness is varied. The monolithic solution is unaffected by this parameter variation and serves as a baseline. For both the D/t ratios, the cladded pipe definitely serve to increase the collapse pressure. The effect was more pronounced for the thinner walled pipe.

Figure 6.6 shows the collapse pressure distribution when the boundary condition of the model is changed. Table 5.1 outlines the different types used. Table 6.2 outlines the boundary condition numbering.

The DNV solution is again unaffected by the choice of boundary condition and serves as a baseline. The monolithic and cladded solutions are both mildy affected by the boundary conditions. The capped end boundary condition yields the highest collapse pressures, while the plane stress yields the lowest. The cladded soulution again displays a strengthening effect across the range and is more pronounced for the higher D/t ratios.

Figure 6.7 shows the collapse pressure distribution when the length factor of

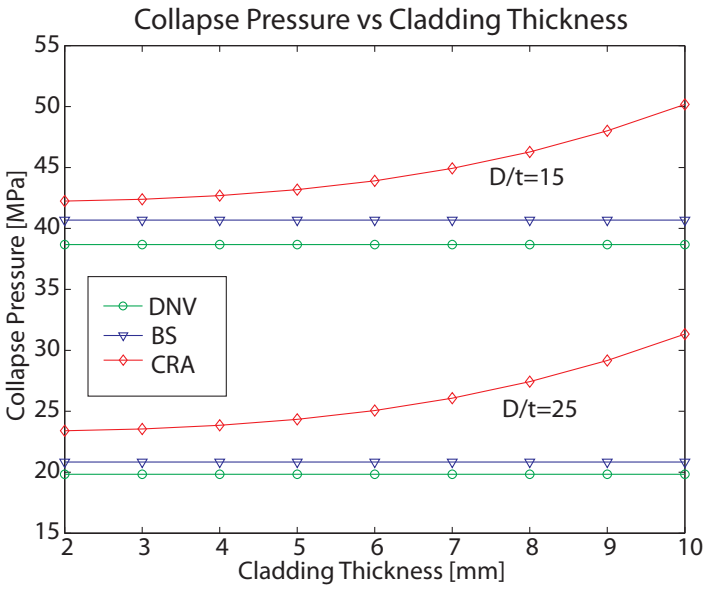

Figure 6.5: Collapse pressure vs cladding thickness

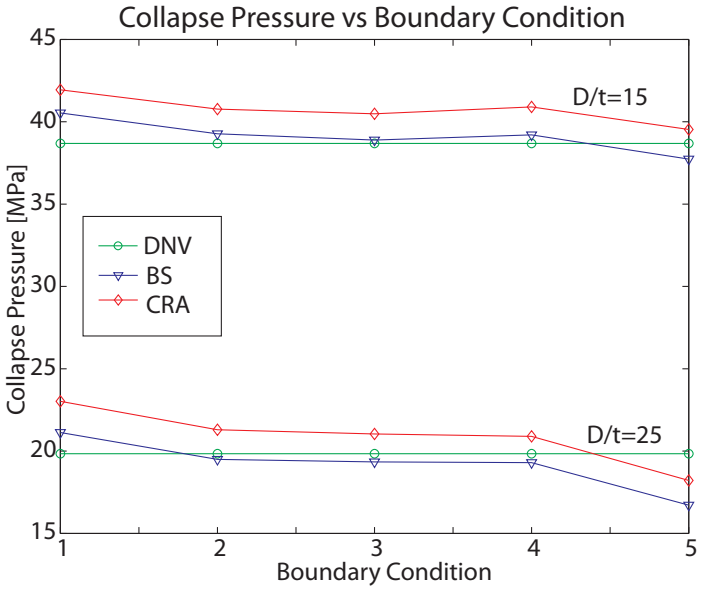

Figure 6.6: Collapse pressure vs boundary condition for monolithic and cladded pipe

Boundary Condition	Number
Capped End	1
Clamped End	2
Infinite Pipeline	3
Plane Strain	4
Plane Stress	5

Table 6.2: Boundary condition reference

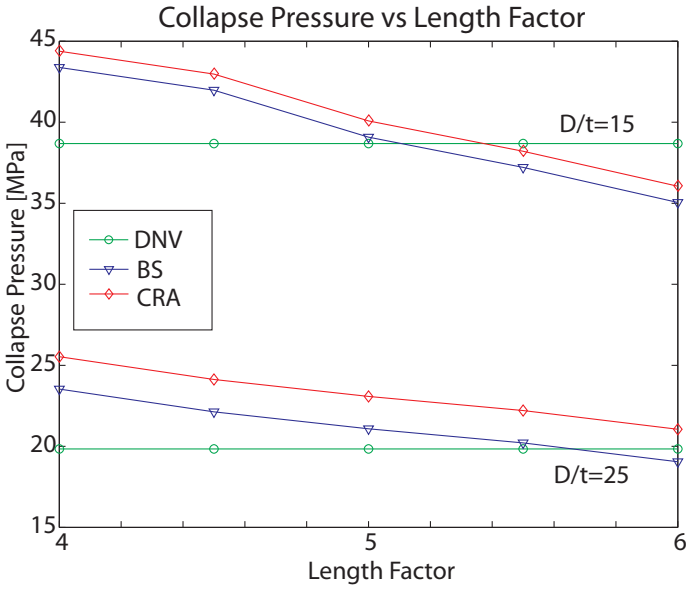

Figure 6.7: Collapse pressure vs length factor for monolithic and cladded pipe

the model is varied. The DNV solution is unaffected by the length of the pipe segment and serves as a baseline. The monolithic solution shows mild response to varying the length factor. The effect begins to flatten out once the length factor reaches $L_p \approx 5$. The strengthening effect of the cladding is observed through out the range, indicating that it is mimicing the collapse mode of the monolithic solution. The strengthening effect is magnified for higher D/t ratios. This behaviour is expected as lengthening the pipe segment will essentially reduce the effect of the end conditions imposed on the pipe.

Material

Applying different material models to the cladding can give some insight into its collapse behaviour.

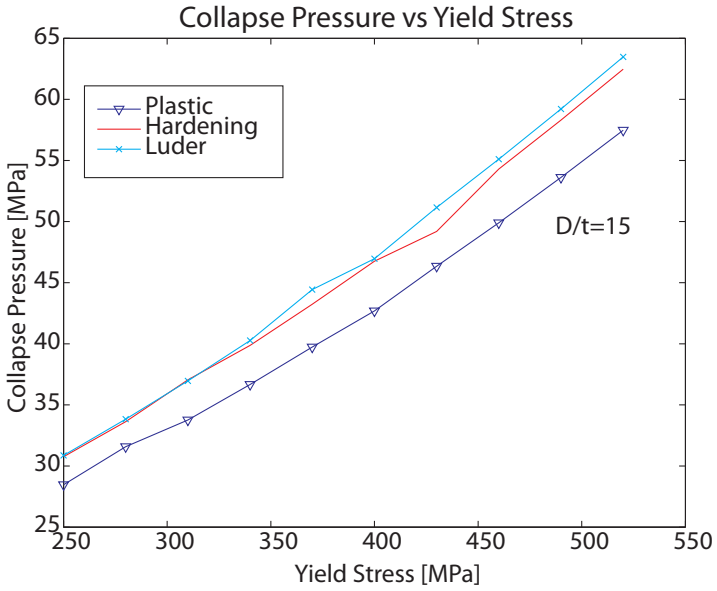

Figure 6.8: Collapse pressure vs yield stress for cladded pipe.

Figure 6.8 shows the collapse pressure distribution when the yield stress of different material models are varied. The perfectly plastic material model is applied to the cladding, which results in a much lower strengthening effect than previously observed. The hardening material model gives a much better strengthening effect than the plastic model, due primarily to the strain hardening that is present in the hardening model. The Luder plateau model yielded very similar results to the hardening model. The results are smooth for the first half of the yield stress range but exhibit some instability towards the end. This corresponds to the few simulations where the Riks method was unable to converge on an equilibrium. Algorithm variables were mildy adjusted to assist in convergence but this may have results in errors higher than tolerated.

Choosing a $D/t = 15$ ratio meant that the pipe segment would collapse plastically. A similar feature of all the material models depicted in figure 6.8 is that the onset of plastic behaviour is not continuous.

Low D/t ratios collapse plastically while high ratios collapse elastically. Equation 6.1 shows the expression for the transition ratio which is clearly

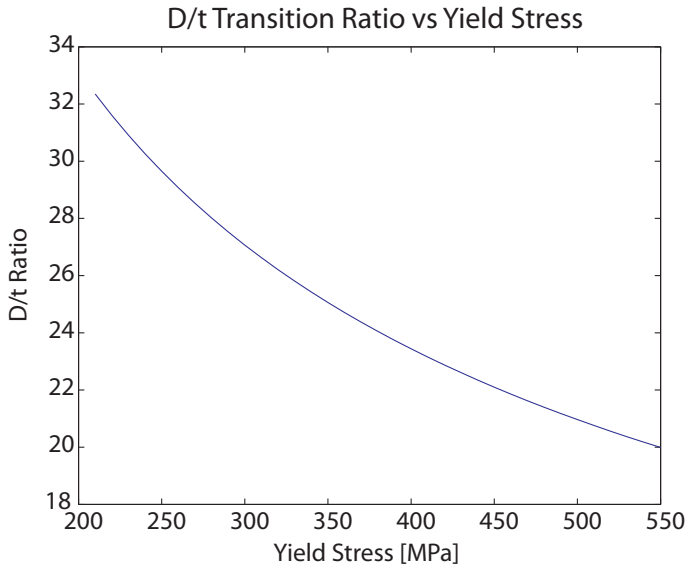

Figure 6.9: Transition D/t ratio vs yield stress

dependant on the E/σ_y ratio. Figure 6.9 shows the transition D/t ratio for different values of yield stress. The choosen values for D/t and yield stress indicate that the majority of simulations are collapsing plastically with the exception of a few simulations with low yield stresses. Considering the application of the pipes, plastic collapse is deemed the most crucial dimensioning criteria.

$$(D/t)_{tr} = \sqrt{\frac{E}{(1-\nu^2)\sigma_y}} \tag{6.1}$$

Figure 6.10 shows the collapse pressure distribution when the Ramberg-Osgood material mode is used with varying yield stress. The fit parameter n is shown for 3 seperate cases and the hardening material model is used as a baseline. When $n = 8$, the material model exhibits a greater strain hardening than compared to other values of n. As expected, when $n = 8$, the response is quite similar to the hardening model with the difference between them increasing as the yield stress increases. The case of when $n = 13$ gave lower results than when $n = 8$ and again shows some erratic response towards end of the yield stress range. The case when $n = 30$ gave the lowest collapse pressure readings but seemed to have an increased response for

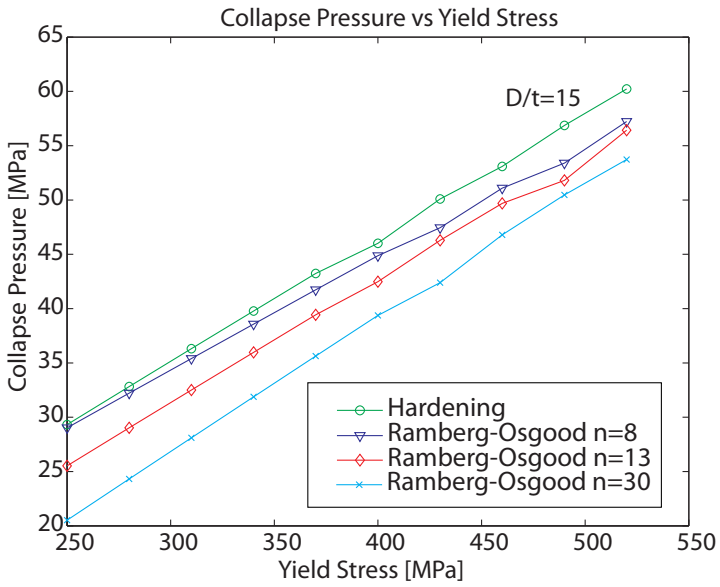

Figure 6.10: Collapse pressure vs yield stress for cladded pipe.

higher yield stresses. This behaviour is expected considering the amount of strain hardening behaviour each of the respective models exhibit. The major advantage of using the Ramberg-Osgood material model is to generate a stress-strain response that is continous between the elastic and plastic parts of the response. This stress-strain response is in close accordance with true stress-strain response of carbon steel.

Figure 6.10 shows the collapse pressure distribution while the initial circumferential stresses are varied. The DNV solution is independant of this parameter so is represented used as a base line. In both cases the monolithic pipe is quite heavily affected by the initial stresses. The strength of the cladded pipe is also noticeably greatly than the monolithic solution except for high initial stresses for the thick walled pipe. When $D/t = 25$, the numerical response is less pronounced than when $D/t = 15$. This behaviour is expected as the main contributor to plastic collapse is the pipes circumferential strength for which large initial stresses will place the material closer to its yield stress. This will then accelerate the onset of plastic circumferential strains.

This provides a result base for the response of monolithic and cladded pipe sections when subject to purely hydrostatic loading.

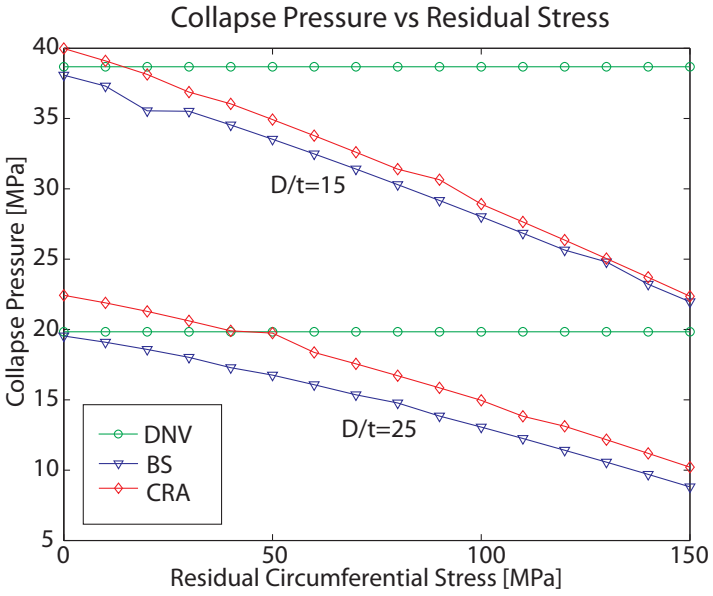

Figure 6.11: Collapse pressure vs Initial circumferential stresses

Chapter 7

Conclusion

7.1 Concluding Remarks

This thesis provides an extensive introduction into the field of subsea pipeline structural intergrity. Execution methodology and comparitive methods can be useful for orientation within problems of a similar nature. A cylindrical coordinate proved to be a good choice for representation of a pipe section. Theory such as bifurcation and non-linearity are presented with an emphasise on critical concepts that are involved in collapse based problems. The premise of a non-linear analysis has been evaluated considering the nature of the problem, and which non-linearities are deemed important.

Desirable features inherent from the production process are summarised, including production techniques that influence collapse pressure. Geometric and residual stresses are found to be the most influential factors resulting from the UOE production process. Implementation of these production byproducts are considered when implementing the numerical solution. A brief discussion of the subsea operations that introduce unique loading situations have been considered. The very nature of hydrostatic loading has revealed some insight into the basis of the non-linear geometry implementation, indicating that the action of the hydrostatic load is always normal to the surface of the pipe. Correlating the numerical model to full scale test procedures is done through consideration of end cap forces.

Current design standards have been compared and used as a baseline during finite element implementation. Keys parameters have been defined in relation to the problem. The DNV solution yielded the best all-round solution so is

used as a baseline for further investigation. Assumptions that govern the behaviour of collapse modes are stated so the actual response can be deemed relevant. Assuming isotropic materail response is motivated by various heat treatment methods that recover majority of the pipes strength.

A detailed description of the finite element adaptation has been defined. Essential parameters have been implemented considering the natural limitations of the thesis. Wall thickness, ovality, eccentricity, pipe length and cladding thickness are the relevant geometric imperfections. Refined definitions of geometric imperfections and material non-linearity have helped to shape solution schemes. A convergence analysis confirms the mesh density necessary for accurate results. Verification of the numerical model has been completed for a three way comparison between the analytic, numerical and experimental results. This has yielded an acceptable numerical model upon which simulations can be performed.

Simulation results, corresponding geometric imperfections and material models are generated. The geometric imperfections chosen for the numerical scheme seemed to have a strong correlation to the collapse capacity. D/t ratio and ovality are the most pronounced, while a weaken degree of response was observed with respect to eccentricity. The thickness of the inner cladding had definte strengthening effect, and also shared similar geometric response compared to the monolithic case.

Implementing different material models allowed for considering the failure mechanism that induces the local buckling. For lower values of D/t ratio, plastic collapse is observed. This means that the material properties transition between elastic and plastic behaviour is an important factor. It is clear that the Ramberg-Osgood model provides the best material model due its continuous transition between elastic and plastic response. Using the Ramberg-Osgood model to simulate the cladded material properties resulted in lower collapse pressure than when compared to other material models, but displayed more stability over the yield stress range.

This emphasises the need for an accurate and continuous material data. The cladded pipe has clearly displayed a strengthening effect for almost all simulations, indicating the need for full scale test data to verify these numerical solutions. The implementation of documentation for the strengthening of cladded pipe allows for designers to dimension accordingly. The cost of pipe production is always of prime concern and can be drastically reduced by this implementation.

7.2 Further Studies

Assumptions that are enforced during this thesis can be reconsidered to further investigate the nature of the problem. Key parameters presented in the paper can subject to cross parameter variation. This will generate a much larger pool of data that can be graphically represented and further discussed.

Material properties can be considered anisotropically from material coupon tests. Further optimisation of the Ramberg-Osgood material model can be performed from an anisotropic point of view. Combined loading situations can be considered as depicted in figure 3.4. This will allow for the collapse capacity to be dimensioned for installation loads.

The bond between the inner cladding can be considered with imperfections. Geometric imperfections of the inner cladding can also be considered independantly from the backing steel.

Appendix A

Appendix

A.1 DNV Collapse Equation

The DNV recommended equation is given as.

$$(p_c - p_{el})\left(p_c^2 - p_{pl}^2\right) = p_c p_{el} p_{pl} f_0 \frac{D_o}{t}$$

This can be interpreted as a third order polynomial where the unknown x is the collapse pressure, p_c.

$$ax^3 + bx^2 + cx + d = 0$$

$$p_c^3 - p_{el}p_c^2 - (p_{pl}^2 + p_{el}p_{pl}f_0\frac{D_o}{t})p_c + p_{el}p_{pl}^2 = 0$$

The analytical solution is given as.

$$p_c = y - \frac{1}{3}b$$

$$b = -p_{el}$$

$$c = \left(p_{pl}^2 + p_{pl}p_{el}f_0\frac{D_o}{t}\right)$$

$$d = p_{el}p_{pl}^2$$

$$u = \frac{1}{3}\left(-\frac{1}{3}b^2 + c\right)$$

$$v = \frac{1}{2}\left(\frac{2}{27}b^3 - \frac{1}{3}bc + d\right)$$

$$\Phi = \arccos\left(\frac{-v}{\sqrt{-u^3}}\right)$$

$$y = -2\sqrt{-u}\cos\left(\frac{\Phi}{3} + \frac{60\pi}{180}\right)$$

A.2 Input Files

The following section will declare the input scripts used to run the finite element simulations.

main_input.inp is main control file that calls upon the different components of the FE model.

```
*HEADING
Clad Pipe Collapse (Jean Louis)
********************************************************************************
********************** Trigger Required Compiler Data *********************************
*PREPRINT,ECHO=NO, PARVALUES=YES, MODEL=NO, CONTACT=NO, HISTORY=YES
*PARAMETER
********************** Primary Geometry of Pipe ***************************************
Dt_ratio=25
outer_diameter=500
pipe_length_factor=5
********************** Ovality Definitions ********************************************
ovality_dir_x=1
ovality_dir_y=0
ovality_percent=1
********************** End Cap Loading ************************************************
end_cap=1
********************** Residual Circumferential Stresses ******************************
residual_max=0
********************** CRA Layer Information ******************************************
CRA_thickness=3
CRA_radial_layers=5
********************** Calculate helper constants *************************************
*INCLUDE, INPUT=helper_constants.inp
********************** Eccentricity  global********************************************
*PARAMETER
eccent_percent_x=0
eccent_percent_y=0
********************** Peaking, flattening and local eccentricity **********************
*PARAMETER
peaking_ratio_inner=0
peaking_ratio_outer=0
********************** Labeling key nodes *********************************************
*INCLUDE, INPUT=key_nodes.inp
********************** Enter Nodal Coordinates ****************************************
```

```
*INCLUDE, INPUT=nodal_coordinates.inp
********************** Use NGEN Command to sweep circumferentially ******************
*INCLUDE, INPUT=nodal_generation.inp
********************** Parameter values for Element connectivity ********************
*INCLUDE, INPUT=key_elements.inp
********************** Element meshing ***********************************************
*INCLUDE, INPUT=element_generation.inp
********************** Create Inner and Outer Surfaces ******************************
*INCLUDE, INPUT=surface_generation.inp
********************** Material Prop *************************************************
*INCLUDE, INPUT=local_system.inp
*PARAMETER
youngs=200.0e3
youngs_CRA=200e3
poisson=0.3
yield_stress=300
yield_stress_CRA=200
yield_stress_luder=yield_stress+1
hardening_factor=0.1
hardening_modulus=hardening_factor*youngs
ultimate=1500.0
ultimate_strain=((ultimate-yield_stress)/hardening_modulus)
plateau_strain_percent=1.0
plateau_strain=plateau_strain_percent/100.0
ultimate_strain_luder=((ultimate-yield_stress)/hardening_modulus)+plateau_strain
*INCLUDE, INPUT=material_BS_Plastic.inp
*INCLUDE,INPUT=material_CRA_Plastic.inp
********************** Contact Condition *********************************************
*INCLUDE, INPUT=contact.inp
********************** Defining Initial Residul Stresses *****************************
*INCLUDE, INPUT=initial_stress.inp
********************** Boundary Conditions and Coupling ******************************
*INCLUDE, INPUT=boundary_capend.inp
********************** Solution Steps ************************************************
*INCLUDE, INPUT=steps.inp
```

helper_constants.inp defines all required helper dimensions necessary.

```
*PARAMETER
radial_layers_BS=5
circum_layers=80
axial_layers=50
extra_angle_circum=8
extra_mesh_circum=8
remain_angle=360-extra_angle_circum
half_angle=extra_angle_circum/2.0
half_remain_angle=360-half_angle
ovality=ovality_percent/100.0
stress_layer_1=residual_max
stress_layer_2=residual_max/2
stress_layer_3=0
stress_layer_4=-residual_max/2
stress_layer_5=-residual_max
outer_radius=outer_diameter/2
total_thickness=outer_diameter/Dt_ratio
thickness_BS=total_thickness
inner_radius=outer_radius-thickness_BS
CRA_radius=inner_radius-CRA_thickness
pipe_length=pipe_length_factor*outer_radius
ovality_x_inner=((1+(ovality/2))*ovality_dir_x)+((1-(ovality/2))*ovality_dir_y)
```

```
ovality_y_inner=((1-(ovality/2))*ovality_dir_x)+((1+(ovality/2))*ovality_dir_y)
x_inner=inner_radius*ovality_x_inner
y_inner=inner_radius*ovality_y_inner
x_outer=x_inner+total_thickness
y_outer=y_inner+total_thickness
ovality_x_outer=x_outer/outer_radius
ovality_y_outer=y_outer/outer_radius
x_CRA=x_inner-CRA_thickness
y_CRA=y_inner-CRA_thickness
ovality_x_CRA=x_CRA/CRA_radius
ovality_y_CRA=y_CRA/CRA_radius
radial_layers=radial_layers_BS
circum_step=720/circum_layers
missing_angle=360-(circum_step/2)
helper_angle=circum_step/2.0
last_angle=360-helper_angle
riks_criteria=(0.25*inner_radius*ovality_dir_x*-1)+(0.25*inner_radius*ovality_dir_y*-1)
outer_area=3.14159*(outer_radius**2)*ovality_x_outer*ovality_y_outer
inner_area=3.14159*(inner_radius**2)*ovality_x_inner*ovality_y_inner
area_dif=outer_area-inner_area
load_ratio=outer_area/area_dif
load_ratio_apply=load_ratio*end_cap
eccent_x=eccent_percent_x*total_thickness*0.5*0.01
eccent_y=eccent_percent_y*total_thickness*0.5*0.01
peaking_center_inner=(total_thickness*0.5)*peaking_ratio_inner
peaking_center_outer=(total_thickness*0.5)*peaking_ratio_outer
radius_peak_inner=inner_radius+peaking_center_inner
radius_peak_outer=outer_radius+peaking_center_outer
radius_peak_CRA=radius_peak_inner-CRA_thickness
```

key_nodes.inp defines all the key nodes required for geometric generation.

```
*PARAMETER
front_center_node=1000
back_center_node=(axial_layers+1)*1000
front_inner_key_0_CRA=101001
front_inner_key_090_CRA=101181
front_inner_key_180_CRA=101361
front_inner_key_270_CRA=101541
front_inner_key_359_CRA=101721-circum_step
front_inner_key_360_CRA=101721
front_inner_extra_start=101801
front_inner_extra_end=101801+extra_mesh_circum
extra_half_mesh=extra_mesh_circum/2
front_inner_extra_mid=101900
front_outer_key_0_BS=front_inner_key_0_CRA+(radial_layers_BS*1000)
front_outer_key_090_BS=front_inner_key_090_CRA+(radial_layers_BS*1000)
front_outer_key_180_BS=front_inner_key_180_CRA+(radial_layers_BS*1000)
front_outer_key_270_BS=front_inner_key_270_CRA+(radial_layers_BS*1000)
front_outer_key_359_BS=front_inner_key_359_CRA+(radial_layers_BS*1000)
front_outer_key_360_BS=front_inner_key_360_CRA+(radial_layers_BS*1000)
front_outer_extra_start=front_inner_extra_start+(radial_layers_BS*1000)
front_outer_extra_end=front_inner_extra_end+(radial_layers_BS*1000)
front_outer_extra_mid=front_inner_extra_mid+(radial_layers_BS*1000)
back_inner_key_0_CRA=front_inner_key_0_CRA+(axial_layers*100000)
back_inner_key_090_CRA=front_inner_key_090_CRA+(axial_layers*100000)
back_inner_key_180_CRA=front_inner_key_180_CRA+(axial_layers*100000)
back_inner_key_270_CRA=front_inner_key_270_CRA+(axial_layers*100000)
back_inner_key_359_CRA=front_inner_key_359_CRA+(axial_layers*100000)
back_inner_key_360_CRA=front_inner_key_360_CRA+(axial_layers*100000)
```

```
back_inner_extra_start=front_inner_extra_start+(axial_layers*100000)
back_inner_extra_end=front_inner_extra_end+(axial_layers*100000)
back_inner_extra_mid=front_inner_extra_mid+(axial_layers*100000)
back_outer_key_0_BS=front_outer_key_0_BS+(axial_layers*100000)
back_outer_key_090_BS=front_outer_key_090_BS+(axial_layers*100000)
back_outer_key_180_BS=front_outer_key_180_BS+(axial_layers*100000)
back_outer_key_270_BS=front_outer_key_270_BS+(axial_layers*100000)
back_outer_key_359_BS=front_outer_key_359_BS+(axial_layers*100000)
back_outer_key_360_BS=front_outer_key_360_BS+(axial_layers*100000)
back_outer_extra_start=front_outer_extra_start+(axial_layers*100000)
back_outer_extra_end=front_outer_extra_end+(axial_layers*100000)
back_outer_extra_mid=front_outer_extra_mid+(axial_layers*100000)
riks_node=(ovality_dir_x*101181)+(ovality_dir_y*101361)
riks_dof=(ovality_dir_x*1)+(ovality_dir_y*1)
CRA_front_inner_0=80101001
CRA_front_inner_090=80101181
CRA_front_inner_180=80101361
CRA_front_inner_270=80101541
CRA_front_inner_359=80101721-circum_step
CRA_front_inner_360=80101721
CRA_front_inner_extra_start=80101801
CRA_front_inner_extra_end=80101801+extra_mesh_circum
CRA_front_inner_extra_mid=80101900
CRA_front_outer_0=80101001+((CRA_radial_layers)*1000)
CRA_front_outer_090=80101181+((CRA_radial_layers)*1000)
CRA_front_outer_180=80101361+((CRA_radial_layers)*1000)
CRA_front_outer_270=80101541+((CRA_radial_layers)*1000)
CRA_front_outer_359=80101721-circum_step+((CRA_radial_layers)*1000)
CRA_front_outer_360=80101721+((CRA_radial_layers)*1000)
CRA_front_outer_extra_start=80101801+((CRA_radial_layers)*1000)
CRA_front_outer_extra_end=80101801+extra_mesh_circum+((CRA_radial_layers)*1000)
CRA_front_outer_extra_mid=80101900+((CRA_radial_layers)*1000)
CRA_back_inner_0=80101001+(axial_layers*100000)
CRA_back_inner_090=80101181+(axial_layers*100000)
CRA_back_inner_180=80101361+(axial_layers*100000)
CRA_back_inner_270=80101541+(axial_layers*100000)
CRA_back_inner_359=80101721-circum_step+(axial_layers*100000)
CRA_back_inner_360=80101721+(axial_layers*100000)
CRA_back_inner_extra_start=80101801+(axial_layers*100000)
CRA_back_inner_extra_end=80101801+extra_mesh_circum+(axial_layers*100000)
CRA_back_inner_extra_mid=80101900+(axial_layers*100000)
CRA_back_outer_0=80101001+(axial_layers*100000)+((CRA_radial_layers)*1000)
CRA_back_outer_090=80101181+(axial_layers*100000)+((CRA_radial_layers)*1000)
CRA_back_outer_180=80101361+(axial_layers*100000)+((CRA_radial_layers)*1000)
CRA_back_outer_270=80101541+(axial_layers*100000)+((CRA_radial_layers)*1000)
CRA_back_outer_359=80101721-circum_step+(axial_layers*100000)+((CRA_radial_layers)*1000)
CRA_back_outer_360=80101721+(axial_layers*100000)+((CRA_radial_layers)*1000)
CRA_back_outer_extra_start=80101801+(axial_layers*100000)+((CRA_radial_layers)*1000)
CRA_back_outer_extra_end=80101801+extra_mesh_circum+(axial_layers*100000)+((CRA_radial_layers)*1000)
CRA_back_outer_extra_mid=80101900+(axial_layers*100000)+((CRA_radial_layers)*1000)
```

nodal_coordinates.inp defines all key nodal coordinates.

```
*NODE, SYSTEM=C
<front_center_node>,0,0,0
<back_center_node>,0,0,<pipe_length>
<front_inner_key_0_CRA>,<inner_radius>,<half_angle>,0
<front_inner_key_090_CRA>,<inner_radius>,90,0
<front_inner_key_180_CRA>,<inner_radius>,180,0
<front_inner_key_270_CRA>,<inner_radius>,270,0
```

<front_inner_key_360_CRA>,<inner_radius>,<half_remain_angle>,0
<front_inner_extra_start>,<inner_radius>,<half_remain_angle>,0
<front_inner_extra_end>,<inner_radius>,<half_angle>,0
<front_inner_extra_mid>,<radius_peak_inner>,0,0
<front_outer_key_0_BS>,<outer_radius>,<half_angle>,0
<front_outer_key_090_BS>,<outer_radius>,90,0
<front_outer_key_180_BS>,<outer_radius>,180,0
<front_outer_key_270_BS>,<outer_radius>,270,0
<front_outer_key_360_BS>,<outer_radius>,<half_remain_angle>,0
<front_outer_extra_start>,<outer_radius>,<half_remain_angle>,0
<front_outer_extra_end>,<outer_radius>,<half_angle>,0
<front_outer_extra_mid>,<radius_peak_outer>,0,0
<back_inner_key_0_CRA>,<inner_radius>,<half_angle>,<pipe_length>
<back_inner_key_090_CRA>,<inner_radius>,90,<pipe_length>
<back_inner_key_180_CRA>,<inner_radius>,180,<pipe_length>
<back_inner_key_270_CRA>,<inner_radius>,270,<pipe_length>
<back_inner_key_360_CRA>,<inner_radius>,<half_remain_angle>,<pipe_length>
<back_inner_extra_start>,<inner_radius>,<half_remain_angle>,<pipe_length>
<back_inner_extra_end>,<inner_radius>,<half_angle>,<pipe_length>
<back_inner_extra_mid>,<radius_peak_inner>,0,<pipe_length>
<back_outer_key_0_BS>,<outer_radius>,<half_angle>,<pipe_length>
<back_outer_key_090_BS>,<outer_radius>,90,<pipe_length>
<back_outer_key_180_BS>,<outer_radius>,180,<pipe_length>
<back_outer_key_270_BS>,<outer_radius>,270,<pipe_length>
<back_outer_key_360_BS>,<outer_radius>,<half_remain_angle>,<pipe_length>
<back_outer_extra_start>,<outer_radius>,<half_remain_angle>,<pipe_length>
<back_outer_extra_end>,<outer_radius>,<half_angle>,<pipe_length>
<back_outer_extra_mid>,<radius_peak_outer>,0,<pipe_length>
<CRA_front_inner_0>,<CRA_radius>,<half_angle>,0
<CRA_front_inner_090>,<CRA_radius>,90,0
<CRA_front_inner_180>,<CRA_radius>,180,0
<CRA_front_inner_270>,<CRA_radius>,270,0
<CRA_front_inner_360>,<CRA_radius>,<half_remain_angle>,0
<CRA_front_inner_extra_start>,<CRA_radius>,<half_remain_angle>,0
<CRA_front_inner_extra_end>,<CRA_radius>,<half_angle>,0
<CRA_front_inner_extra_mid>,<radius_peak_CRA>,0,0
<CRA_front_outer_0>,<inner_radius>,<half_angle>,0
<CRA_front_outer_090>,<inner_radius>,90,0
<CRA_front_outer_180>,<inner_radius>,180,0
<CRA_front_outer_270>,<inner_radius>,270,0
<CRA_front_outer_360>,<inner_radius>,<half_remain_angle>,0
<CRA_front_outer_extra_start>,<inner_radius>,<half_remain_angle>,0
<CRA_front_outer_extra_end>,<inner_radius>,<half_angle>,0
<CRA_front_outer_extra_mid>,<radius_peak_inner>,0,0
<CRA_back_inner_0>,<CRA_radius>,<half_angle>,<pipe_length>
<CRA_back_inner_090>,<CRA_radius>,90,<pipe_length>
<CRA_back_inner_180>,<CRA_radius>,180,<pipe_length>
<CRA_back_inner_270>,<CRA_radius>,270,<pipe_length>
<CRA_back_inner_360>,<CRA_radius>,<half_remain_angle>,<pipe_length>
<CRA_back_inner_extra_start>,<CRA_radius>,<half_remain_angle>,<pipe_length>
<CRA_back_inner_extra_end>,<CRA_radius>,<half_angle>,<pipe_length>
<CRA_back_inner_extra_mid>,<radius_peak_CRA>,0,<pipe_length>
<CRA_back_outer_0>,<inner_radius>,<half_angle>,<pipe_length>
<CRA_back_outer_090>,<inner_radius>,90,<pipe_length>
<CRA_back_outer_180>,<inner_radius>,180,<pipe_length>
<CRA_back_outer_270>,<inner_radius>,270,<pipe_length>
<CRA_back_outer_360>,<inner_radius>,<half_remain_angle>,<pipe_length>
<CRA_back_outer_extra_start>,<inner_radius>,<half_remain_angle>,<pipe_length>
<CRA_back_outer_extra_end>,<inner_radius>,<half_angle>,<pipe_length>
<CRA_back_outer_extra_mid>,<radius_peak_inner>,0,<pipe_length>

nodal_generation.inp defines all geometric imperfections.

```
*NGEN, NSET=INSIDEFRONT, LINE=C, SYSTEM=C
<front_inner_key_0_CRA>,<front_inner_key_090_CRA>,<circum_step>,<front_center_node>
<front_inner_key_090_CRA>,<front_inner_key_180_CRA>,<circum_step>,<front_center_node>
<front_inner_key_180_CRA>,<front_inner_key_270_CRA>,<circum_step>,<front_center_node>
<front_inner_key_270_CRA>,<front_inner_key_360_CRA>,<circum_step>,<front_center_node>
*NMAP, NSET=INSIDEFRONT, TYPE=SCALE, DEFINITION=NODES
<front_center_node>
<ovality_x_inner>,<ovality_y_inner>,1
*NGEN, NSET=INSIDEEXTRA, LINE=P,SYSTEM=C
<front_inner_extra_start>,<front_inner_extra_end>,1,<front_inner_extra_mid>
*NMAP, NSET=INSIDEEXTRA, TYPE=SCALE, DEFINITION=NODES
<front_center_node>
<ovality_x_inner>,<ovality_y_inner>,1
*NGEN, NSET=INSIDEFRONT_CRA, LINE=C, SYSTEM=C
<CRA_front_inner_0>,<CRA_front_inner_090>,<circum_step>,<front_center_node>
<CRA_front_inner_090>,<CRA_front_inner_180>,<circum_step>,<front_center_node>
<CRA_front_inner_180>,<CRA_front_inner_270>,<circum_step>,<front_center_node>
<CRA_front_inner_270>,<CRA_front_inner_360>,<circum_step>,<front_center_node>
*NMAP, NSET=INSIDEFRONT_CRA, TYPE=SCALE, DEFINITION=NODES
<front_center_node>
<ovality_x_CRA>,<ovality_y_CRA>,1
*NGEN, NSET=INSIDEEXTRA_CRA, LINE=P,SYSTEM=C
<CRA_front_inner_extra_start>,<CRA_front_inner_extra_end>,1,<CRA_front_inner_extra_mid>
*NMAP, NSET=INSIDEEXTRA_CRA, TYPE=SCALE, DEFINITION=NODES
<front_center_node>
<ovality_x_CRA>,<ovality_y_CRA>,1
*NGEN, NSET=INSIDEBACK, LINE=C, SYSTEM=C
<back_inner_key_0_CRA>,<back_inner_key_090_CRA>,<circum_step>,<back_center_node>
<back_inner_key_090_CRA>,<back_inner_key_180_CRA>,<circum_step>,<back_center_node>
<back_inner_key_180_CRA>,<back_inner_key_270_CRA>,<circum_step>,<back_center_node>
<back_inner_key_270_CRA>,<back_inner_key_360_CRA>,<circum_step>,<back_center_node>
*NMAP, NSET=INSIDEBACK, TYPE=SCALE, DEFINITION=NODES
<back_center_node>
<ovality_x_inner>,<ovality_y_inner>,1
*NGEN, NSET=INSIDEEXTRABACK, LINE=P,SYSTEM=C
<back_inner_extra_start>,<back_inner_extra_end>,1,<back_inner_extra_mid>
*NMAP, NSET=INSIDEEXTRABACK, TYPE=SCALE, DEFINITION=NODES
<back_center_node>
<ovality_x_inner>,<ovality_y_inner>,1
*NGEN, NSET=INSIDEBACK_CRA, LINE=C, SYSTEM=C
<CRA_back_inner_0>,<CRA_back_inner_090>,<circum_step>,<back_center_node>
<CRA_back_inner_090>,<CRA_back_inner_180>,<circum_step>,<back_center_node>
<CRA_back_inner_180>,<CRA_back_inner_270>,<circum_step>,<back_center_node>
<CRA_back_inner_270>,<CRA_back_inner_360>,<circum_step>,<back_center_node>
*NMAP, NSET=INSIDEBACK_CRA, TYPE=SCALE, DEFINITION=NODES
<back_center_node>
<ovality_x_CRA>,<ovality_y_CRA>,1
*NGEN, NSET=INSIDEEXTRABACK_CRA, LINE=P,SYSTEM=C
<CRA_back_inner_extra_start>,<CRA_back_inner_extra_end>,1,<CRA_back_inner_extra_mid>
*NMAP, NSET=INSIDEEXTRABACK_CRA, TYPE=SCALE, DEFINITION=NODES
<back_center_node>
<ovality_x_CRA>,<ovality_y_CRA>,1
*NGEN, NSET=OUTSIDEFRONT, LINE=C, SYSTEM=C
<front_outer_key_0_BS>,<front_outer_key_090_BS>,<circum_step>,<front_center_node>
<front_outer_key_090_BS>,<front_outer_key_180_BS>,<circum_step>,<front_center_node>
<front_outer_key_180_BS>,<front_outer_key_270_BS>,<circum_step>,<front_center_node>
<front_outer_key_270_BS>,<front_outer_key_360_BS>,<circum_step>,<front_center_node>
*NMAP, NSET=OUTSIDEFRONT, TYPE=SCALE, DEFINITION=NODES
<front_center_node>
```

```
<ovality_x_outer>,<ovality_y_outer>,1
*NGEN, NSET=OUTSIDEEXTRA, LINE=P,SYSTEM=C
<front_outer_extra_start>,<front_outer_extra_end>,1,<front_outer_extra_mid>
*NMAP, NSET=OUTSIDEEXTRA, TYPE=SCALE, DEFINITION=NODES
<front_center_node>
<ovality_x_outer>,<ovality_y_outer>,1
*NSET, NSET=OUTSIDEFRONT
OUTSIDEFRONT,OUTSIDEEXTRA
*NMAP, NSET=OUTSIDEFRONT, TYPE=RECTANGULAR, DEFINITION=COORDINATES
<eccent_x>,<eccent_y>,0
*NGEN, NSET=OUTSIDEFRONT_CRA, LINE=C, SYSTEM=C
<CRA_front_outer_0>,<CRA_front_outer_090>,<circum_step>,<front_center_node>
<CRA_front_outer_090>,<CRA_front_outer_180>,<circum_step>,<front_center_node>
<CRA_front_outer_180>,<CRA_front_outer_270>,<circum_step>,<front_center_node>
<CRA_front_outer_270>,<CRA_front_outer_360>,<circum_step>,<front_center_node>
*NMAP, NSET=OUTSIDEFRONT_CRA, TYPE=SCALE, DEFINITION=NODES
<front_center_node>
<ovality_x_inner>,<ovality_y_inner>,1
*NGEN, NSET=OUTSIDEEXTRA_CRA, LINE=P,SYSTEM=C
<CRA_front_outer_extra_start>,<CRA_front_outer_extra_end>,1,<CRA_front_outer_extra_mid>
*NMAP, NSET=OUTSIDEEXTRA_CRA, TYPE=SCALE, DEFINITION=NODES
<front_center_node>
<ovality_x_inner>,<ovality_y_inner>,1
*NSET, NSET=OUTSIDEFRONT_CRA
OUTSIDEFRONT_CRA,OUTSIDEEXTRA_CRA
*NGEN, NSET=OUTSIDEBACK, LINE=C, SYSTEM=C
<back_outer_key_0_BS>,<back_outer_key_090_BS>,<circum_step>,<back_center_node>
<back_outer_key_090_BS>,<back_outer_key_180_BS>,<circum_step>,<back_center_node>
<back_outer_key_180_BS>,<back_outer_key_270_BS>,<circum_step>,<back_center_node>
<back_outer_key_270_BS>,<back_outer_key_360_BS>,<circum_step>,<back_center_node>
*NMAP, NSET=OUTSIDEBACK, TYPE=SCALE, DEFINITION=NODES
<back_center_node>
<ovality_x_outer>,<ovality_y_outer>,1
*NGEN, NSET=OUTSIDEEXTRABACK, LINE=P,SYSTEM=C
<back_outer_extra_start>,<back_outer_extra_end>,1,<back_outer_extra_mid>
*NMAP, NSET=OUTSIDEEXTRABACK, TYPE=SCALE, DEFINITION=NODES
<back_center_node>
<ovality_x_outer>,<ovality_y_outer>,1
*NSET,NSET=OUTSIDEBACK
OUTSIDEBACK, OUTSIDEEXTRABACK
*NMAP, NSET=OUTSIDEBACK, TYPE=RECTANGULAR, DEFINITION=COORDINATES
<eccent_x>,<eccent_y>,0
*NGEN, NSET=OUTSIDEBACK_CRA, LINE=C, SYSTEM=C
<CRA_back_outer_0>,<CRA_back_outer_090>,<circum_step>,<back_center_node>
<CRA_back_outer_090>,<CRA_back_outer_180>,<circum_step>,<back_center_node>
<CRA_back_outer_180>,<CRA_back_outer_270>,<circum_step>,<back_center_node>
<CRA_back_outer_270>,<CRA_back_outer_360>,<circum_step>,<back_center_node>
*NMAP, NSET=OUTSIDEBACK_CRA, TYPE=SCALE, DEFINITION=NODES
<back_center_node>
<ovality_x_inner>,<ovality_y_inner>,1
*NGEN, NSET=OUTSIDEEXTRABACK_CRA, LINE=P,SYSTEM=C
<CRA_back_outer_extra_start>,<CRA_back_outer_extra_end>,1,<CRA_back_outer_extra_mid>
*NMAP, NSET=OUTSIDEEXTRABACK_CRA, TYPE=SCALE, DEFINITION=NODES
<back_center_node>
<ovality_x_inner>,<ovality_y_inner>,1
*NSET,NSET=OUTSIDEBACK_CRA
OUTSIDEBACK_CRA, OUTSIDEEXTRABACK_CRA
*NSET, NSET=INSIDEFRONT
INSIDEFRONT,INSIDEEXTRA
*NFILL, NSET=FRONT_BS
INSIDEFRONT,OUTSIDEFRONT, <radial_layers_BS>, 1000
*NSET, NSET=INSIDEFRONT_CRA
```

```
INSIDEFRONT_CRA,INSIDEEXTRA_CRA
*NFILL, NSET=FRONT_CRA
INSIDEFRONT_CRA,OUTSIDEFRONT_CRA, <CRA_radial_layers>, 1000
*NSET, NSET=INSIDEBACK
INSIDEBACK, INSIDEEXTRABACK
*NFILL, NSET=BACK_BS
INSIDEBACK,OUTSIDEBACK, <radial_layers_BS>, 1000
*NSET, NSET=INSIDEBACK_CRA
INSIDEBACK_CRA, INSIDEEXTRABACK_CRA
*NFILL, NSET=BACK_CRA
INSIDEBACK_CRA,OUTSIDEBACK_CRA, <CRA_radial_layers>, 1000
*NSET,NSET=FRONT_ALLNODES
FRONT_BS,FRONT_CRA
*NSET,NSET=BACK_ALLNODES
BACK_BS,BACK_CRA
*NFILL, NSET=ALLNODES
FRONT_ALLNODES,BACK_ALLNODES,<axial_layers>,100000
*TRANSFORM, NSET=ALLNODES, TYPE=C
0,0,0,0,0,1
*NSET,NSET=BACK_CENTER
<back_center_node>
```

key_elements.inp defines all key element labels.

```
*PARAMETER
helper_circum_elements=circum_layers
first_element_BS=101001
helper_A_BS=front_inner_key_0_CRA
helper_B_BS=front_inner_key_0_CRA+circum_step
helper_C_BS=helper_B_BS+100000
helper_D_BS=helper_A_BS+100000
helper_E_BS=helper_A_BS+1000
helper_F_BS=helper_B_BS+1000
helper_G_BS=helper_F_BS+100000
helper_H_BS=helper_E_BS+100000
helper_I_BS=front_inner_key_360_CRA
helper_J_BS=helper_I_BS+100000
helper_K_BS=helper_I_BS+1000
helper_L_BS=helper_J_BS+1000
last_element_BS=first_element_BS+circum_layers-1
helper_circum_extra=extra_mesh_circum-2
first_element_extra=101801
helper_A_extra=101721
helper_B_extra=101802
helper_C_extra=201802
helper_D_extra=201721
helper_E_extra=102721
helper_F_extra=102802
helper_G_extra=202802
helper_H_extra=202721
second_element_extra=101802
helper_A_extra_2=101802
helper_B_extra_2=101803
helper_C_extra_2=201803
helper_D_extra_2=201802
helper_E_extra_2=102802
helper_F_extra_2=102803
helper_G_extra_2=202803
helper_H_extra_2=202802
last_element_extra=101801+helper_circum_extra+1
```

```
helper_A_extra_3=front_inner_extra_end-1
helper_B_extra_3=front_inner_key_0_CRA
helper_C_extra_3=helper_B_extra_3 + 100000
helper_D_extra_3=helper_A_extra_3 + 100000
helper_E_extra_3=helper_A_extra_3 + 1000
helper_F_extra_3=helper_B_extra_3 + 1000
helper_G_extra_3=helper_F_extra_3 + 100000
helper_H_extra_3=helper_E_extra_3 + 100000
first_layer_1=first_element_BS
last_layer_1=last_element_BS
first_layer_2=first_layer_1+1000
last_layer_2=last_layer_1+1000
first_layer_3=first_layer_2+1000
last_layer_3=last_layer_2+1000
first_layer_4=first_layer_3+1000
last_layer_4=last_layer_3+1000
first_layer_5=first_layer_4+1000
last_layer_5=last_layer_4+1000
first_element_CRA=80101001
helper_A_CRA=CRA_front_inner_0
helper_B_CRA=CRA_front_inner_0+circum_step
helper_C_CRA=helper_B_CRA+100000
helper_D_CRA=helper_A_CRA+100000
helper_E_CRA=helper_A_CRA+1000
helper_F_CRA=helper_B_CRA+1000
helper_G_CRA=helper_F_CRA+100000
helper_H_CRA=helper_E_CRA+100000
radial_CRA_M1=CRA_radial_layers-1
first_element_extra_CRA=80101801
helper_A_extra_CRA=80101721
helper_B_extra_CRA=80101802
helper_C_extra_CRA=80201802
helper_D_extra_CRA=80201721
helper_E_extra_CRA=80102721
helper_F_extra_CRA=80102802
helper_G_extra_CRA=80202802
helper_H_extra_CRA=80202721
second_element_extra_CRA=80101802
helper_A_extra_2_CRA=80101802
helper_B_extra_2_CRA=80101803
helper_C_extra_2_CRA=80201803
helper_D_extra_2_CRA=80201802
helper_E_extra_2_CRA=80102802
helper_F_extra_2_CRA=80102803
helper_G_extra_2_CRA=80202803
helper_H_extra_2_CRA=80202802
last_element_extra_CRA=80101801+helper_circum_extra+1
helper_A_extra_3_CRA=CRA_front_inner_extra_end-1
helper_B_extra_3_CRA=CRA_front_inner_0
helper_C_extra_3_CRA=helper_B_extra_3_CRA + 100000
helper_D_extra_3_CRA=helper_A_extra_3_CRA + 100000
helper_E_extra_3_CRA=helper_A_extra_3_CRA + 1000
helper_F_extra_3_CRA=helper_B_extra_3_CRA + 1000
helper_G_extra_3_CRA=helper_F_extra_3_CRA + 100000
helper_H_extra_3_CRA=helper_E_extra_3_CRA + 100000
last_help=last_element_extra_CRA+(radial_CRA_M1*1000)
last_help_A=helper_A_extra_3_CRA+(radial_CRA_M1*1000)
last_help_B=helper_B_extra_3_CRA+(radial_CRA_M1*1000)
last_help_C=helper_C_extra_3_CRA+(radial_CRA_M1*1000)
last_help_D=helper_D_extra_3_CRA+(radial_CRA_M1*1000)
```

element_generation.inp defines all element connectivity.

```
*ELEMENT, TYPE=C3D8R, ELSET=LAYER_1
<first_layer_1>,<helper_A_BS>,<helper_B_BS>,<helper_C_BS>,<helper_D_BS>,
<helper_E_BS>,<helper_F_BS>,<helper_G_BS>,<helper_H_BS>
*ELGEN,ELSET=LAYER_1
<first_layer_1>,<helper_circum_elements>,<circum_step>,1,<axial_layers>,100000,100000
*ELEMENT, TYPE=C3D8R, ELSET=LAYER_2
<first_layer_2>,102001,102010,202010,202001,
103001,103010,203010,203001
*ELGEN,ELSET=LAYER_2
<first_layer_2>,<helper_circum_elements>,<circum_step>,1,<axial_layers>,100000,100000
*ELEMENT, TYPE=C3D8R, ELSET=LAYER_3
<first_layer_3>,103001,103010,203010,203001,
104001,104010,204010,204001
*ELGEN,ELSET=LAYER_3
<first_layer_3>,<helper_circum_elements>,<circum_step>,1,<axial_layers>,100000,100000
*ELEMENT, TYPE=C3D8R, ELSET=LAYER_4
<first_layer_4>,104001,104010,204010,204001,
105001,105010,205010,205001
*ELGEN,ELSET=LAYER_4
<first_layer_4>,<helper_circum_elements>,<circum_step>,1,<axial_layers>,100000,100000
*ELEMENT, TYPE=C3D8R, ELSET=LAYER_5
<first_layer_5>,105001,105010,205010,205001,
106001,106010,206010,206001
*ELGEN,ELSET=LAYER_5
<first_layer_5>,<helper_circum_elements>,<circum_step>,1,<axial_layers>,100000,100000
*ELEMENT, TYPE=C3D8R, ELSET=ELEM_CRA
<first_element_CRA>,<helper_A_CRA>,<helper_B_CRA>,<helper_C_CRA>,<helper_D_CRA>,
<helper_E_CRA>,<helper_F_CRA>,<helper_G_CRA>,<helper_H_CRA>
*ELGEN,ELSET=ELEM_CRA
<first_element_CRA>,<helper_circum_elements>,<circum_step>,1,<radial_CRA_M1>,1000,1000,
<axial_layers>,100000,100000
*ELEMENT, TYPE=C3D8R, ELSET=ELEM_CRA
80105001,80105001,80105010,80205010,80205001,101001,101010,201010,201001
*ELGEN, ELSET=ELEM_CRA
80105001,<helper_circum_elements>,<circum_step>,1,<axial_layers>,100000,100000
*ELEMENT,TYPE=C3D8R,ELSET=EXTRA
<first_element_extra>,<helper_A_extra>,<helper_B_extra>,<helper_C_extra>,<helper_D_extra>,
<helper_E_extra>,<helper_F_extra>,<helper_G_extra>,<helper_H_extra>
<second_element_extra>,<helper_A_extra_2>,<helper_B_extra_2>,<helper_C_extra_2>,<helper_D_extra_2>,
<helper_E_extra_2>,<helper_F_extra_2>,<helper_G_extra_2>,<helper_H_extra_2>
<last_element_extra>,<helper_A_extra_3>,<helper_B_extra_3>,<helper_C_extra_3>,<helper_D_extra_3>,
<helper_E_extra_3>,<helper_F_extra_3>,<helper_G_extra_3>,<helper_H_extra_3>
*ELGEN,ELSET=EXTRA
<second_element_extra>,<helper_circum_extra>,1,1,<radial_layers_BS>,1000,1000,
<axial_layers>,100000,100000
*ELGEN,ELSET=EXTRA
<first_element_extra>,<radial_layers_BS>,1000,1000,<axial_layers>,100000,100000
*ELGEN,ELSET=EXTRA
<last_element_extra>,<radial_layers_BS>,1000,1000,<axial_layers>,100000,100000
*ELEMENT,TYPE=C3D8R,ELSET=EXTRA_CRA
<first_element_extra_CRA>,<helper_A_extra_CRA>,<helper_B_extra_CRA>,
<helper_C_extra_CRA>,<helper_D_extra_CRA>,
<helper_E_extra_CRA>,<helper_F_extra_CRA>,<helper_G_extra_CRA>,<helper_H_extra_CRA>
<second_element_extra_CRA>,<helper_A_extra_2_CRA>,<helper_B_extra_2_CRA>,
<helper_C_extra_2_CRA>,<helper_D_extra_2_CRA>,
<helper_E_extra_2_CRA>,<helper_F_extra_2_CRA>,<helper_G_extra_2_CRA>,<helper_H_extra_2_CRA>
<last_element_extra_CRA>,<helper_A_extra_3_CRA>,<helper_B_extra_3_CRA>,
<helper_C_extra_3_CRA>,<helper_D_extra_3_CRA>,
<helper_E_extra_3_CRA>,<helper_F_extra_3_CRA>,<helper_G_extra_3_CRA>,<helper_H_extra_3_CRA>
```

```
*ELGEN,ELSET=EXTRA_CRA
<second_element_extra_CRA>,<helper_circum_extra>,1,1,<radial_CRA_M1>,1000,1000,
<axial_layers>,100000,100000
*ELGEN,ELSET=EXTRA_CRA
<first_element_extra_CRA>,<radial_CRA_M1>,1000,1000,<axial_layers>,100000,100000
*ELGEN,ELSET=EXTRA_CRA
<last_element_extra_CRA>,<radial_CRA_M1>,1000,1000,<axial_layers>,100000,100000
*ELEMENT,TYPE=C3D8R,ELSET=EXTRA_CRA
80105801,80105721,80105802,80205802,80205721,
101721,101802,201802,201721
80105802,80105802,80105803,80205803,80205802,
101802,101803,201803,201802
<last_help>,<last_help_A>,<last_help_B>,<last_help_C>,<last_help_D>,
<helper_A_extra_3>,<helper_A_BS>,<helper_D_BS>,<helper_D_extra_3>
*ELGEN,ELSET=EXTRA_CRA
80105802,<helper_circum_extra>,1,1,<axial_layers>,100000,100000
*ELGEN,ELSET=EXTRA_CRA
80105801,<axial_layers>,100000,100000
*ELGEN,ELSET=EXTRA_CRA
<last_help>,<axial_layers>,100000,100000
*ELSET, ELSET=MONITOR_LAYER_1,GENERATE
101041,5101041,100000
101061,5101061,100000
*ELSET, ELSET=MONITOR_LAYER_2,GENERATE
102041,5102041,100000
102061,5102061,100000
*ELSET, ELSET=MONITOR_LAYER_3,GENERATE
103041,5103041,100000
103061,5103061,100000
*ELSET, ELSET=MONITOR_LAYER_4,GENERATE
104041,5104041,100000
104061,5104061,100000
*ELSET, ELSET=MONITOR_LAYER_5,GENERATE
105041,5105041,100000
105061,5105061,100000
*ELSET,ELSET=MONITOR
MONITOR_LAYER_1,MONITOR_LAYER_2,MONITOR_LAYER_3,
MONITOR_LAYER_4,MONITOR_LAYER_5
*ELSET,ELSET=BS
LAYER_1,LAYER_2,LAYER_3,LAYER_4,LAYER_5,EXTRA
*ELSET, ELSET=ELEM_CRA
ELEM_CRA,EXTRA_CRA
*ELSET,ELSET=EALL
ELEM_CRA,BS
```

surface_generation.inp defines surfaces of the model.

```
*SURFACE, NAME=SURFACE_S2, TYPE=ELEMENT
BS, S2
*SURFACE, NAME=SURFACE_S3, TYPE=ELEMENT
BS, S3
*SURFACE, NAME=SURFACE_S5, TYPE=ELEMENT
BS, S5
*SURFACE, NAME=SURFACE_S1, TYPE=ELEMENT
ELEM_CRA, S1
*SURFACE, NAME=TEST, TYPE=ELEMENT
EALL
*SURFACE, NAME=EXTERIOR_CORRECT, COMBINE=INTERSECTION
TEST,SURFACE_S2
*SURFACE, NAME=INTERIOR_CORRECT, COMBINE=INTERSECTION
```

```
TEST,SURFACE_S1
*SURFACE, NAME=BACK_FACE_CORRECT, COMBINE=INTERSECTION
TEST,SURFACE_S5
*SURFACE, NAME=FRONT_FACE_CORRECT, COMBINE=INTERSECTION
TEST,SURFACE_S3
```

local_system.inp defines the cyclindrical coordinate system.

```
\textbf{local\_system.inp} defines the cyclindrical coordinate system.
\scriptsize
\begin{verbatim}
*ORIENTATION, NAME=CYLINDRICAL_SYSTEM, DEFINITION=NODES, SYSTEM=CYLINDRICAL
<front_center_node>,<back_center_node>
```

material_BS(CRA).inp defines the material properties. An individual file is created for each material model. The appropriate model must be included. Stress and strains are defined in true values.

```
*SOLID SECTION, ELSET=BS, MATERIAL=BACKINGSTEEL
*MATERIAL, NAME=BACKINGSTEEL
*DENSITY
7.85E-09
*ELASTIC
<youngs>, <poisson>
*PLASTIC, HARDENING=ISOTROPIC
<yield_stress>,0
```

contact.inp defines the inner contact condition.

```
*CONTACT PAIR, INTERACTION=INNER_CONTACT, TYPE=SURFACE TO SURFACE
SURFACE_S1
*SURFACE INTERACTION, NAME=INNER_CONTACT
```

initial_stress.inp initial circumferential stresses.

```
*INITIAL CONDITIONS, TYPE=STRESS, UNBALANCED STRESS=STEP
LAYER_1,0,<stress_layer_1>,0,0,0,0
LAYER_2,0,<stress_layer_2>,0,0,0,0
LAYER_3,0,<stress_layer_3>,0,0,0,0
LAYER_4,0,<stress_layer_4>,0,0,0,0
LAYER_5,0,<stress_layer_5>,0,0,0,0
```

boundary.inp defines the boundary condition and coupling constraint. A seperate input file is created for each case. Below is the capped end boundary condition.

```
*BOUNDARY
<back_center_node>,1,2,0
<back_center_node>,4,6,0
FRONT_ALLNODES, ZSYMM
*COUPLING, CONSTRAINT NAME=COUPLING_BC, REF NODE=<back_center_node>,
SURFACE=BACK_FACE_CORRECT, ORIENTATION=CYLINDRICAL_SYSTEM
*KINEMATIC
1,6
```

steps.inp defines the prestep where actual residual stresses are recording and the hydrostatic loading.

```
*STEP, NLGEOM=YES, NAME=Pre Step
*STATIC
*EL PRINT, ELSET=MONITOR
S
*EL PRINT, ELSET=MONITOR
E
*EL PRINT, ELSET=MONITOR
LE
*EL PRINT, ELSET=MONITOR
EE
*EL PRINT, ELSET=MONITOR
PE
*END STEP
*STEP, NLGEOM=YES, NAME=RIKS Loading Step
*STATIC, RIKS
 , , , , ,<riks_node>,<riks_dof>,<riks_criteria>
*DSLOAD
EXTERIOR_CORRECT, P, 1
BACK_FACE_CORRECT, P, <load_ratio_apply>
*END STEP
```

Bibliography

[1] Glencoe, *Earth Science*
McGraw Hill, Ohio, 2002

[2] Dassault Systems,ABAQUS User Manual (V6.7)
Analysis Section, 2007

[3] Dassault Systems,ABAQUS User Manual (V6.7)
Analysis Section, 2007

[4] Dassault Systems,ABAQUS User Manual (V6.7)
Theory Section, 2007

[5] Dassault Systems,ABAQUS User Manual (V6.7)
Verification Section, 2007

[6] Dassault Systems,ABAQUS User Manual (V6.7)
Benchmark Section, 2007

[7] Kyriakides and Corona, 'Mechanics of Offshore Pipelines'
Elsevier, 2007

[8] Benham, Crawford and Armstrong, 'Mechanics of Engineering Materials'
Prentice Hall, 1996

[9] Det Norske Veritas, 'DNV Offshore Standard DNV-OS-F101'
October 2007

[10] Fyrileiv and Collberg, 'Influence of Pressure in Pipeline Design-Effective Axial Force'
Proceedings of OMAE2005, Norway, 2005

[11] Fallqvist, 'Collapse of thick deepwater pipelines due to hydrostatic pressure'
Masters Thesis, KTH Sweden, 2009

[12] Concepts and Applications of the Finite Element Analysis
Robert D. Cook, David S. Malkus, Michael E. Plesha, Robert J. Witt

[13] DeGeer, Timms, and Lobanov, 'Blue Stream Collapse Test Program'
Proceedings of OMAE2005, 2005

[14] Fryer, Tait, Kyriakides, Timms and DeGeer, 'The Prediction and Enhancement of UOE-DSAW Collapse Resistance for Deepwater Linepipe'
Proceedings of IPC2004, 2004

[15] Stark and McKeehan, 'Hydrostatic Collapse Research in Support of the Oman India Gas Pipeline'
Proceedings of OTC1995, 1995

[16] Tsuru and Asahi, 'Methodology for Measurement of Mechanical Properties to Predict Collapse Pressure of UOE Pipes'
Proceedings of IPC2007, 2007

[17] Toscano, Timms, Dvorkin and DeGeer, 'Determination of the Collapse and Propagation Pressure of Ultra-Deepwater Pipelines'
Proceedings of OMAE2003, 2003

[18] Tsuru and Asahi, 'Collapse Pressure Prediction and Measurement Methodology of UOE Pipe'
Proceedings of IPC2003, 2003

[19] Gresnight, van Foeken and Chen, 'Collapse of UOE Manufactured Steel Pipes'
Proceedings of IPC2000, 2000